

# High-dimensional fractionalization and spinon deconfinement in pyrochlore antiferromagnets

Z. Nussinov,<sup>1</sup> C. D. Batista,<sup>2</sup> B. Normand,<sup>3</sup> and S. A. Trugman<sup>2</sup>

<sup>1</sup>*Department of Physics, Washington University, Compton Hall, 1 Brookings Drive, St. Louis, Missouri 63130, USA*

<sup>2</sup>*Theoretical Division, Los Alamos National Laboratory, Los Alamos, New Mexico 87545, USA*

<sup>3</sup>*Centro Atómico Bariloche and Instituto Balseiro, Comisión Nacional de Energía Atómica, 8400 Bariloche, Argentina*

(Received 1 March 2006; revised manuscript received 29 November 2006; published 9 March 2007)

The ground states of Klein-type spin models on the pyrochlore and checkerboard lattice are spanned by the set of singlet dimer coverings and thus possess an extensive ground-state degeneracy. Among the many exotic consequences is the presence of deconfined fractional excitations (spinons), which propagate through the entire system. While a realistic electronic model on the pyrochlore lattice is close to the Klein point, this point is, in fact, inherently unstable because any perturbation  $\epsilon$  restores spinon confinement at  $T=0$ . We demonstrate that deconfinement is recovered in the finite-temperature region  $\epsilon \ll T \ll J$ , where the deconfined phase can be characterized as a dilute Coulomb gas of thermally excited spinons. We investigate the zero-temperature phase diagram away from the Klein point by means of a variational approach based on the singlet dimer coverings of the pyrochlore lattices and by taking into account their nonorthogonality. We find that in these systems, nearest-neighbor exchange interactions do not lead to Rokhsar-Kivelson-type processes.

DOI: 10.1103/PhysRevB.75.094411

PACS number(s): 75.10.-b, 75.50.Ee, 75.40.Cx, 73.43.Nq

## I. INTRODUCTION

Discovering new phases of matter is a primary objective of physics. The fractionalized spin liquid in two spatial dimensions ( $d=2$ ) has provided a popular candidate framework for models describing the exotic properties observed in many strongly correlated electronic materials, including frustrated quantum magnets and high- $T_c$  superconductors.<sup>1</sup> The spin-liquid state is characterized by spinon excitations carrying a unit charge under a compact  $U(1)$  gauge field. However, Polyakov has argued<sup>2</sup> that a pure compact  $U(1)$  gauge theory is always confining at zero temperature for  $d=2$ , with confinement between test particles with opposite charges being produced by the proliferation of instanton tunneling events.

By contrast, the case for confinement by instanton proliferation in spin systems is rather more involved,<sup>3,4</sup> and the situation at a critical point offers additional possibilities. These considerations underlie a recent discussion of the deconfined quantum critical point<sup>5</sup> as the foundation for the emergence of spin-liquid phases with fractional excitations. However, while this set of elegant ideas appears most plausible, it is not yet clear from any analytical or numerical calculations that there exists a microscopic Hamiltonian, and particularly one with only simple electronic interactions, exemplifying this class of physical phenomena. Quasiparticle fractionalization has been demonstrated rigorously in one dimension (1D) and in the quantum Hall effect. For frustrated quantum spin systems, recent progress was made in the context of a two-dimensional model with high degeneracy in the ground-state manifold, which exhibits (partial) dimensional reduction<sup>6</sup> and consequent spinon deconfinement.<sup>7</sup> We will expand upon and systematize these ideas to provide a further demonstration of a class of physical systems displaying fractional excitations.

To this end, we begin with the natural question of whether a dilute gas of deconfined spinons can be stabilized in dimensions  $d > 1$  in a finite region of the phase diagram. This

latter requirement is crucial for observing deconfined spinon excitations in real systems. We will provide an affirmative answer by considering a highly frustrated  $S=1/2$  model on the  $d=2$  (checkerboard) and  $d=3$  pyrochlore lattices. We demonstrate that for  $T=0$ , the spinon excitations are deconfined at the Klein critical point, whose nature we will explain in detail. As expected from above, this zero-temperature deconfined phase is unstable under any realistic perturbation characterized by an energy scale  $\epsilon$ . We argue that in the regime  $\epsilon \ll J$ , where  $J$  is the characteristic energy scale of the model, a dilute Coulomb gas of spinons is stabilized in the temperature range  $\epsilon \ll T \ll J$ . This result raises the possibility of observing spinons in real higher-dimensional systems.

The checkerboard and pyrochlore lattices (Fig. 1), which form the focus of our analysis, have long been known to possess a geometry which is amenable to very large ground-state degeneracies. The pyrochlore lattice is composed of corner-sharing tetrahedra, arranged in a cubic (fcc) structure, such that each vertex is common to two four-site units [see panel (b) of Fig. 1]. This geometry is rather common in transition-metal and rare-earth oxide systems, specifically in the pyrochlore (the origin of the name) and spinel structures. The pyrochlore systems<sup>8</sup> have chemical formula  $A_2B_2O_7$ , where both  $A$  and  $B$  may be taken from a wide range of

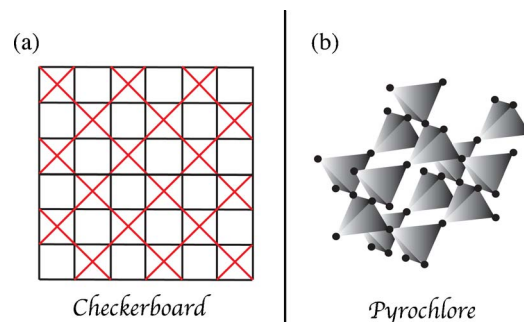


FIG. 1. (Color online) (a) Checkerboard and (b) pyrochlore lattices.

metal ions, particularly rare earths, and both occur on a pyrochlore lattice. Spinel systems<sup>9</sup> have chemical formula  $AB_2O_4$ , where it is more typical for the  $A$  and  $B$  ions to be transition metals and only the  $B$  sites form a pyrochlore structure. Individual compounds in these classes are usually strongly insulating and of fixed ionic valences, and the presence of nonmagnetic ions on one of the sublattices (the  $A$  sites for the spinel) leads to a pyrochlore lattice of interacting spins on the other. It was noted at a very early stage<sup>10,11</sup> that the connectivity of such a structure is not dissimilar to the arrangement found in water ice, a point that we will both explain and exploit extensively below.

The checkerboard lattice can be considered as a two-dimensional (2D) version of the pyrochlore structure, in the sense that it also is composed of corner-sharing tetrahedral units, these being represented by the crossed plaquettes (the terminology we adopt henceforth) in panel (a) of Fig. 1. It is the relatively low coordination number and tetrahedral connectivity of the checkerboard and pyrochlore lattices, which permit a proliferation of ground states. Some of the essential considerations are presented for classical pyrochlore antiferromagnets in Ref. 12 and for quantum pyrochlore antiferromagnets in Ref. 13. While a significant body of recent work has led to a better understanding of icelike phases in pyrochlore ferromagnets,<sup>14</sup> the situation for both classical and quantum antiferromagnets remains far from satisfactory, to the extent that certain results conflict.<sup>15</sup> Here, we provide a further contribution to the body of knowledge concerning quantum pyrochlore antiferromagnets.

We will demonstrate further that the highly unconventional properties listed above arise within simple, nearest-neighbor, bilinear and biquadratic spin models on the 2D and three-dimensional (3D) pyrochlore lattices. These models are derived directly from half-filled, nearest-neighbor Hubbard models, i.e., from models with Coulomb interactions of the shortest range, and are thus fully realistic for electronic systems. The key features giving rise to exotic behavior are (i) an exponential number of degenerate ground states; (ii) exact critical behavior with an emergent divergent correlation length, accompanied by the absence of a long-ranged order; (iii) fractionalization of excited spin states into spinons, which freely propagate in space, implying a separation of spin and charge upon doping these systems (we will show that the emergent fractionalized excitations have well-defined quantum numbers, which may be described as residing at the ends of strings obeying simple rules); (iv) an effective dimensional reduction occurring precisely at the critical point; and (v) topological order in a sense, which we will define explicitly below. All of these features lead in combination with a distinct type of critical point whose static and dynamic properties we will characterize in detail, illustrating, in addition, their connection to a multitude of ideas and concepts emerging in the recent literature in the context of deconfinement and criticality.

In Sec. II, we introduce the type of spin model displaying a Klein point, and discuss its foundation in the electronic Hamiltonian of real, correlated insulating materials. In Sec. III, we begin our analysis of the model at the Klein critical point and at zero temperature, focusing on the characteristic properties here and illustrating their origin in the extensive

ground-state degeneracy. In Sec. IV, we remain at the Klein point but consider finite temperatures to derive the effective entropic interaction of spinon excitations and thus demonstrate their thermally driven deconfinement. In Secs. V and VI, we restore some of the perturbing effects present in the realistic Hamiltonian of Sec. II. Working at zero temperature, in Sec. V, we introduce and apply a specifically constructed variational procedure based on the (nonorthogonal) dimer coverings of the ground-state manifold to demonstrate the selection of specific valence-bond orderings as the ground states of the perturbed system. In Sec. VI, we extend our considerations to finite temperatures and present one example of an exactly critical regime. These calculations indicate explicitly both the confinement of spinons at low temperatures and their liberation at higher temperatures, thus reinforcing the results of Secs. III and IV. Section VII contains a discussion and conclusion.

## II. MODEL

The spin model upon which we focus is a  $S=1/2$  Hamiltonian on the checkerboard and pyrochlore lattices,

$$H = J \sum_{\langle ij \rangle, \alpha} H_{ij}^\alpha + K \sum_{\alpha} (H_{ij}^\alpha H_{kl}^\alpha + H_{il}^\alpha H_{jk}^\alpha + H_{ik}^\alpha H_{jl}^\alpha), \quad (1)$$

where  $\langle ij \rangle$  denotes all pairs of sites in the tetrahedron,  $\alpha \equiv ijkl$ , and  $H_{ij}^\alpha = \vec{S}_i^\alpha \cdot \vec{S}_j^\alpha$  is a scalar product of the two spins. On the checkerboard lattice,  $\alpha$  denotes each crossed plaquette, by which is meant those in Fig. 1(a) with cross-coupling interactions, and the first term is equivalent to both nearest- and next-neighbor Heisenberg interactions of strength  $J$ . This model was considered on the square lattice (all plaquettes crossed) by two of the present authors,<sup>7</sup> and we will contrast the two  $d=2$  systems below. The Heisenberg interaction on the tetrahedral units (we will also refer to the crossed plaquettes of the checkerboard lattice as tetrahedra) of the  $d=2$  and  $d=3$  pyrochlore lattices is strongly frustrated, and the symmetric four-spin interaction pushes the model to maximal frustration at  $K_c = 4J/5$ .<sup>30</sup>

A straightforward but important observation is that  $H$  may be recast in the form

$$H = \frac{J_1}{2} \sum_{\boxtimes} \vec{S}_{\boxtimes}^2 + \frac{J_2}{4} \sum_{\boxtimes} \vec{S}_{\boxtimes}^4, \quad (2)$$

with  $\vec{S}_{\boxtimes}$  the net spin of the tetrahedral unit  $\boxtimes$ ,

$$\vec{S}_{\boxtimes} \equiv \sum_{i \in \boxtimes} \vec{S}_i, \quad (3)$$

$J_1 = J - 7K/4$ , and  $J_2 = K/2$ .<sup>31</sup> This Hamiltonian (1) can be obtained from the Hubbard model on the pyrochlore or checkerboard lattice,

$$H_{\text{Hubb}} = -t \sum_{\langle ij \rangle, \sigma} c_{i\sigma}^\dagger c_{j\sigma} + U \sum_i n_{i\uparrow} n_{i\downarrow}, \quad (4)$$

where  $n_{i\sigma} = c_{i\sigma}^\dagger c_{i\sigma}$  is the number operator for electrons of spin  $\sigma$ . This is perhaps the simplest possible description of interacting electrons with only nearest-neighbor hopping  $t$  and a

local Coulomb repulsion  $U$ . Systems, which are half-filled and have strong on-site interactions are localized insulators where, with the exception of virtual processes, the kinetic energy gain from hopping is sacrificed to avoid the Coulomb cost of double occupancy. The effective Hamiltonian obtained from the virtual hopping processes at the lowest (second) order in the small parameter  $t/U$  is a nearest-neighbor Heisenberg model of the type contained in the first term of Eq. (2), with  $J_1=4t^2/U$  and electronic spin  $\vec{S}_i^a=c_{i\beta}^\dagger\sigma_{\beta\gamma}^a c_{i\gamma}$  ( $a=x,y,z$ ).

A fourth-order strong-coupling expansion of Eq. (4) returns interaction terms bilinear in spins on the same and on different tetrahedra and those biquadratic in spins on the same tetrahedron.<sup>32</sup> As shown in detailed studies performed for plaquettes of the square lattice in the context of planar cuprates,<sup>33</sup> and verified by fits to magnon dispersion relations for the same systems,<sup>34</sup> the latter interactions are stronger than the former by approximately one order of magnitude. Specifically, a far larger number of intratetrahedron processes, whose sum has the symmetric form contained in the second term of Eq. (1), contribute to the effective fourth-order Hamiltonian than processes of the next-neighbor Heisenberg type do. Thus, by retaining only the intratetrahedron processes to fourth order in  $t$ , one obtains the spin Hamiltonian of Eq. (2) with<sup>35</sup>

$$J_1 = \frac{4t^2}{U} - \frac{160t^4}{U^3} + \mathcal{O}\left(\frac{t^6}{U^5}\right),$$

$$J_2 = \frac{40t^4}{U^3} + \mathcal{O}\left(\frac{t^6}{U^5}\right). \quad (5)$$

The general,  $SU(2)$ -invariant spin Hamiltonian arising from a realistic electronic model may thus be considered as an intraplaquette interacting system of exactly the form given in Eq. (2), with only very weak perturbations from intertetrahedron terms. To quantify this statement, in the half-filled system, Eqs. (2) and (4) are related by

$$\tilde{H}_{\text{Hubb}} = H + J_3 \sum_{\langle\langle ij \rangle\rangle} \vec{S}_i \cdot \vec{S}_j, \quad (6)$$

where  $\tilde{H}_{\text{Hubb}}$  is the effective spin Hamiltonian obtained from a fourth-order strong-coupling expansion of  $H_{\text{Hubb}}$ . The sum is over pairs of sites  $\langle\langle i,j \rangle\rangle$  separated by two bonds and which do not belong to the same tetrahedron. The exchange coupling  $J_3$  is given by

$$J_3 = \frac{4t^4}{U^3} + \mathcal{O}\left(\frac{t^6}{U^5}\right). \quad (7)$$

It is evident from Eqs. (5) and (7) that for small  $t/U$ , the interplaquette corrections ( $J_3$ ) originating from the Hubbard Hamiltonian are indeed one order of magnitude smaller than the intraplaquette terms of  $H$  [Eq. (2)].

In Sec. III, we will analyze the properties of Eq. (2) at the Klein point,  $J_1=-J_2$  (Ref. 36) or  $K=K_c=4J/5$ , where the semipositive definite Hamiltonian of Eq. (2) attains its minimal value (when  $S_{\boxtimes}=0$  or 1 on every tetrahedron). The Klein point is quasieactly solvable. (Its ground states may be de-

termined exactly.) Following the observations in the preceding paragraph, in Secs. V and VI, we will expand our treatment to include perturbations around the Klein point, which are of two types: the stronger, represented by nearest-neighbor Heisenberg terms, corresponds to deviations of Eq. (1) from the point  $K=K_c$  and the weaker, represented by next-neighbor Heisenberg terms (and, for the checkerboard, cyclic terms on the uncrossed plaquettes), corresponds to fourth-order interplaquette interactions. Specific  $S=1/2$  materials can be expected at least in the 3D pyrochlore structure, such as that formed by the magnetic ions at both  $A^{m+}$  and  $B^{n+}$  ( $m+n=7$ ) sites in the stereotypical pyrochlore systems  $A_2B_2O_7$  and on the  $B$  sites in  $A^{m+}B_2^{n+}O_4$  ( $m+2n=8$ ) spinels. However, despite the considerable choice of magnetic and nonmagnetic ionic species afforded by these two structural classes, to date we are not aware of the successful synthesis of any such compounds, which maintain the full cubic lattice symmetry.

### III. EXACT GROUND STATES FOR THE $S=1/2$ SYSTEM AT THE KLEIN POINT

Equation (2) suggests an even simpler way of expressing the Hamiltonian,

$$H = \sum_{\boxtimes} h_{\boxtimes}, \quad (8)$$

with  $h_{\boxtimes}$  a quartic polynomial in the total spin of the four sites forming a given tetrahedral unit of the pyrochlore lattice,  $h_{\boxtimes} = \frac{1}{2}J_1 S_{\boxtimes}^2 + \frac{1}{4}J_2 S_{\boxtimes}^4$ . For clarity, we provide a brief review of the possible two- and four-particle states of  $S=1/2$  spins. For a system of four coupled spins, the total spin  $S_{\boxtimes}$  of any tetrahedron obeys  $0 \leq S_{\boxtimes} \leq 2$ . The 16-state spin space is decomposed into two singlet states ( $S_{\boxtimes}=0$ ), three triplets ( $S_{\boxtimes}=1$ ), and one quintet ( $S_{\boxtimes}=2$ ) as follows:

$$\frac{1}{2} \otimes \frac{1}{2} \otimes \frac{1}{2} \otimes \frac{1}{2} = 0 \oplus 0 \oplus 1 \oplus 1 \oplus 2. \quad (9)$$

In this explicit decomposition, the right-hand side labels the disjoint net spin ( $S_{\boxtimes}$ ) sectors while the left-hand side encodes the 16-dimensional space spanned by the direct product of the four  $S=1/2$  particles. The sum of any two nearest-neighbor spins on the lattice,  $(\vec{S}_i + \vec{S}_j)^2 = S_{\text{pair}}(S_{\text{pair}}+1)$ , takes only the two values  $S_{\text{pair}}=0,1$ . If any two spins within a given tetrahedron are in a singlet state ( $S_{\text{pair}}=0$ ), then the total spin of this tetrahedron cannot exceed unity,  $S_{\boxtimes} \leq 1$ . For the parameter choice  $K=K_c$  ( $J_2=-J_1$ ),  $H$  [Eq. (2)] can be rewritten, up to irrelevant constants, as a Klein Hamiltonian<sup>37</sup>

$$H_K = \frac{12}{5}J \sum_{\boxtimes} \mathcal{P}_{\boxtimes}, \quad (10)$$

where  $\mathcal{P}$  is the projection operator onto the subspace of net spin  $S_{\boxtimes}=2$ .

Next, we note, following Ref. 39, that because the number of lattice sites is double the number of tetrahedra,  $N_s=2N_t$ , the set of ground states with one singlet per tetrahedron can

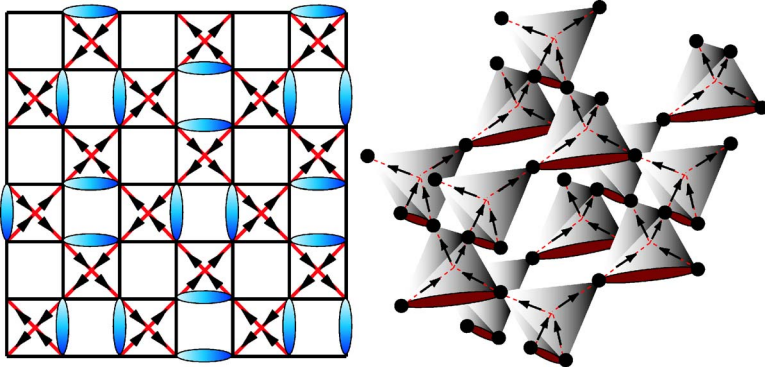


FIG. 2. (Color online) Highly regular ground states on the checkerboard and pyrochlore lattices. The ovals denote singlet dimer states. The arrows denote the representations of these dimer states within the six-vertex model (see text). On each plaquette (tetrahedron), the dimer connects the bases of the two incoming arrows.

be mapped onto the set of hard-core dimer coverings of the lattice. Thus, any dimer covering of the lattice with precisely one dimer per tetrahedron is a ground state of  $H_K$ . Further, any state  $|\psi\rangle$ , which is a superposition of dimer coverings, each of which has one dimer per tetrahedron,

$$|\psi\rangle = \sum_P \alpha_P \prod_{ij \in P} |S_{ij}\rangle \quad \text{with } |S_{ij}\rangle = \frac{1}{\sqrt{2}}(|\uparrow\downarrow\rangle - |\downarrow\uparrow\rangle) \quad (11)$$

(the dimer coverings are labeled by  $P$ ), is also a ground state of  $H_K$ . One of the simplest ground states is afforded by the dimer coverings depicted in Fig. 2. While it is clear that any state of the form of Eq. (11) is a ground state, a proof that all ground states are of this form is far less obvious. It may, nevertheless, be shown rigorously<sup>38</sup> that for Klein models on the pyrochlore lattices, all ground states are indeed of the type specified in Eq. (11).

As a first qualitative consequence of this result, it was noted in Ref. 7 for the analogous point in the square-lattice Hamiltonian that satisfying this constraint leads to a significant degeneracy because dimer singlets may be rearranged along diagonal lines of the lattice with no energy cost. The ground-state entropy scales with the perimeter of the system, and pairs of single-spin (spinon) excitations on the diagonal lines have no binding energy for any separation. Thus, the effective dimensional reduction from 2D to 1D leads to the presence of deconfined spinons whose propagation is essentially unidimensional. On the pyrochlore lattice, the open structure of crossed plaquettes creates a less constrained system, and the number of dimer configurations in the ground-state manifold is strongly enhanced, with the still more massive degeneracy implying similarly exotic physics in this case. We proceed quantitatively by computing the ground-state entropy in Sec. III A.

In addition to the simple coverings shown in Fig. 2, a far richer variety of states exists. The mapping onto the spin-ice problem mentioned briefly above provides a useful classification of these ground states. We stress that the states with one dimer per tetrahedral unit defined by Eq. (11) map exactly to the ice problem,<sup>14,16</sup> where, motivated by the structure of H atoms in solid water,<sup>10,11</sup> two of the sites of any elementary unit (a tetrahedron) are associated with an incoming arrow pointing toward the center of the tetrahedron and two sites lie on the arrows pointing outwards. We label the two sites belonging to a singlet dimer  $|S_{ij}\rangle$  in a given tetrahedron  $\boxtimes \equiv ijkl$  by two incoming arrows from sites  $i$  and  $j$  to the

center of the unit  $\boxtimes \equiv ijkl$ . In this fashion, it is clear that the system is mapped to a set of continuous directed lines such that each tetrahedral unit has exactly two incoming and two outgoing arrows relative to its center. An example of this mapping is illustrated in Fig. 2. A longer but ultimately equivalent version of this mapping, enabling a study of correlations and degeneracies, was reported in Ref. 39. The mapping is one to one: any spin-ice configuration determines a unique singlet-covering state with one dimer per tetrahedral unit and vice versa. The conservation of incoming and outgoing arrows in the spin-ice representation is the foundation for the divergence-free condition we will employ below. Throughout this work, we focus on systems with periodic boundary conditions (PBCs). A system with open boundary conditions (OBCs) would possess a number of additional ground states not captured by the six-vertex mapping, the entropy of which scales like the system surface.

### A. Ground-state degeneracy and entropy

Because the number of pyrochlore spin-ice states is bounded from below<sup>40</sup> by the Pauling limit,<sup>11</sup> the number of ground states (or, more precisely, of nonorthogonal dimer coverings) is given by

$$N_g > (3/2)^{N/2}, \quad (12)$$

with  $N$  the number of vertices of the pyrochlore lattice and  $N_g$  the number of ground-state singlet dimer coverings. We emphasize that this degeneracy is exponential in the system volume, yielding an extensive entropy with a simple, analytical expression for the lower bound, the Pauling entropy  $S_P = \frac{1}{2} N k_B \ln \frac{3}{2}$ . The “exact” entropy of the ice problem is known from series expansion methods,<sup>41</sup> which yield the numerical result

$$S_g = (0.205\,01\,\dots) N k_B > S_P = (0.202\,73\,\dots) N k_B. \quad (13)$$

Similarly, for the checkerboard lattice, the system is reduced to the exact spin-ice model<sup>42</sup> on the square lattice formed by the centers of the crossed plaquettes, leading to an exact singlet-dimer-covering degeneracy<sup>42,43</sup> of

$$N_g = (4/3)^{3N/4}, \quad (14)$$

with  $N$  the number of vertices of the checkerboard lattice, whence  $S_g = \frac{3}{4} N k_B \ln \frac{4}{3}$ . In this derivation, we have assumed that the singlet dimer coverings, although nonorthogonal, are

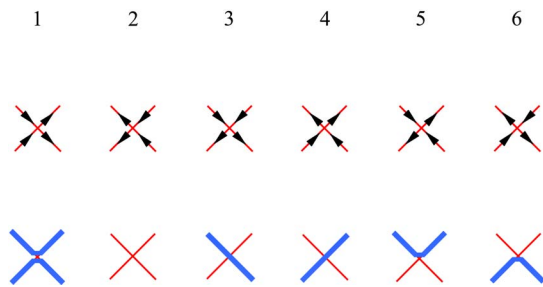


FIG. 3. (Color online) Standard representation of six-vertex states in terms of lines (Ref. 42). Every line is composed of links whose arrows point to the right in the vertex representation.

linearly independent.<sup>44</sup> There are additional “defect” states in the ground-state manifold, in which two singlet dimers may occupy a single tetrahedron, or unpaired spins may be present, without altering the total energy.<sup>46</sup> However, because the entropy of these states scales with the system surface, they constitute a set of measure zero in comparison with the extensive set of dimer coverings, and will be neglected in what follows.

### B. Geometry of ground states

To examine the structure of general ground states of the model [Eq. (1)] at the Klein point, we invoke the line representation of the six-vertex model<sup>42</sup> depicted in Fig. 3. In this convention, every line is composed of links whose arrows point to the right, and there is clear one-to-one mapping between the six-vertex and the line representations. An essential property of the lines is their “chiral” nature: they always represent a motion only to the right (Fig. 3). We will show in detail below (Fig. 7) that this chirality is not merely an artificial feature of the line representation, but it encodes the physical restrictions on the possible spinon paths in the background of the allowed dimer states.

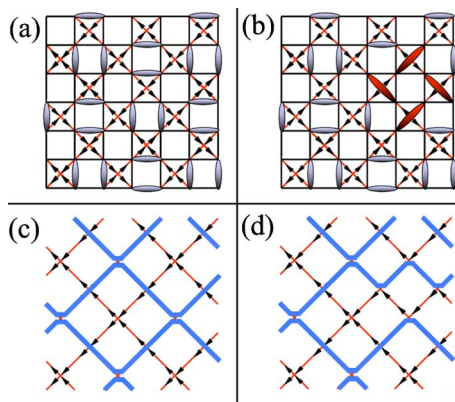


FIG. 4. (Color online) Left: representation of six-vertex states in a highly regular dimer configuration (a) in terms of lines (c). Joining the vertex coverings according to the standard prescription (see text) (Ref. 42) allows one to label all permitted ground states. Right: an elementary local spin interaction process, leading to another dimer configuration (b), corresponds to flipping one of the line corners in the line representation (d).

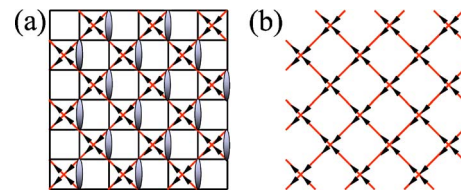


FIG. 5. (Color online) Uniform dimer covering or ferroelectric state (Ref. 42), corresponding to vacuum of lines. The opposing ferroelectric polarization obtained by spatial inversion corresponds to the state which is full of lines.

Finding the elementary process connecting a given dimer covering with other ground states is straightforward in the line representation. Figure 4(c) shows the line representation of the ground state depicted in Fig. 2. The simplest process in the dimer basis corresponds to flipping over one of the line corners in the line representation, as depicted in Figs. 4(c) and 4(d). Note that there is an uncrossed plaquette (in the original lattice) associated with each such corner flip. Returning to the dimer representation, such a process corresponds to a cyclic rotation of the four dimers connected to the uncrossed plaquette [Fig. 4(b)]. A similar process around a hexagon whose edges belong to six different tetrahedra is obtained for the pyrochlore lattice. For clarity of explanation, we comment that in Figs. 4(c) and 4(d), and later in this section, the six-vertex (thin lines with arrows) and line representations (thick) are superposed to aid in illustrating their equivalence, but either alone is a complete representation of the system in terms of independent sets of quantum numbers.

The mapping to the line representation shows that the low-energy sector of a Hamiltonian at the Klein point can be mapped into a string model. It is clear that the total number of lines is a conserved quantity under any local physical process, where by “local” we mean that the process changes only a finite number of (spin) degrees of freedom. The dimer coverings may therefore be classified according to this line quantum number. As an example, in Fig. 5 we show that the uniform or “ferroelectric”<sup>42</sup> dimer covering corresponds to the vacuum of lines. The number conservation implies that this state cannot be connected with any other ground states by a local process. The other ferroelectric dimer state (of opposite polarization), which is obtained by spatial inversion, corresponds to the state, which is full of lines in the line representation, and by the same argument is not connected by a local process to any other states in the ground manifold. Spatial inversion corresponds to the line-antiline transformation (line conjugation) in the line representation.

Not unexpectedly, the exact solution of the six-vertex model<sup>42</sup> reveals that the ground states of greatest importance (by which is meant those becoming increasingly sharp in the thermodynamic limit) are those containing, on a checkerboard lattice of size  $L \times L$ , precisely  $L/2$  lines. This sector has the highest statistical (entropic) weight by virtue of the many ground states it possesses. Analogously, we will see in Sec. V that when the system is perturbed away from the Klein point at  $T=0$ , the state stabilized by the perturbation is generally one with  $L/2$  lines.<sup>47</sup>

### C. Critical correlations

To expand upon the previous statements, we stress that all of the dimer coverings in the ground-state manifold are in-

dividually eigenstates of the Hamiltonian. Thus, there are no quantum fluctuations at the Klein point, and a zero-temperature transition through this point, for example, as a function of  $K/J$ , is a discontinuous, first-order quantum phase transition.<sup>7</sup> The Klein point is a distinct type of critical point, which is essentially classical in nature with critical thermal fluctuations at all temperatures  $T > 0$ .

It has long been known<sup>42</sup> that the square-lattice ice model formed by the centers of the crossed plaquettes in the checkerboard lattice exhibits critical power-law correlations, which have been investigated extensively in Refs. 17. Elementary entropic arguments combined with the ice condition lead to a simple dipolar analogy suggesting that the dimer correlations in  $d$  dimensions exhibit an  $|r|^{-d}$  decay, where  $\mathbf{r}$  is the separation between dimers.<sup>17</sup> Specifically, denoting by  $\mathbf{P}=(\pm 1, 0, 0)$  the first two six-vertex configurations of Fig. 3, and similarly by  $\mathbf{P}=(0, \pm 1, 0)$  and  $\mathbf{P}=(0, 0, \pm 1)$  the other two pairs, the line representation applied for the pyrochlore lattice yields<sup>17</sup>

$$\langle P_i(0)P_j(r) \rangle = \frac{A}{r^3} [\delta_{ij} - 3\hat{r}_i\hat{r}_j] \quad (15)$$

for large separation  $|r|$ , with  $i, j=1, 2, 3$  denoting the spatial components of  $\mathbf{P}$ ,  $\hat{\mathbf{r}}$  the unit vector in the direction of  $\mathbf{r}$ , and  $A$  a constant. The correlation function for the checkerboard lattice has a similar  $|r|^{-2}$  decay. When interpreted as flux lines, the six-vertex arrows (Fig. 3) adhere at every vertex to a strict condition of no divergence. This correspondence, along with the entropic arguments, underlies the dipolar correlations. The zero-flux condition at every vertex leads to the long-ranged correlations (in fact, with infinite correlation length) of the dimers.

The ground-state manifold at  $K=K_c$  corresponds to the high-temperature limit of the ice model, in which every six-vertex configuration is realized with equal amplitude. As such,<sup>42</sup> the system is in the “disordered” critical phase described earlier, where, in particular, the expectation value of any local six-vertex order parameter vanishes.<sup>42</sup> On the checkerboard (pyrochlore) lattice, the different sets of states in the manifold remain characterized by the net number of vertical lines on each horizontal row (plane) of lattice sites (or conversely): this number is conserved and corresponds to a topologically invariant “flux” of lines. Because lines of arrows cannot terminate in the six-vertex representation the flux cannot change from one plane to the next in the pyrochlore.<sup>42</sup> We remark for clarity that for the checkerboard lattice the “horizontal” and “vertical” directions specified above for the dual lattice are rotated by  $45^\circ$  relative to the horizontal and vertical directions of the original lattice. Although the system does not possess local order, it displays this elementary topological order characterized by the topologically invariant flux.<sup>48</sup> The model discussed here forms a high-dimensional realization of Wen’s string nets.<sup>48</sup> On the checkerboard lattice, conservation of the line quantum number means that if  $n_Y$  is the number of vertical lines intercepting a horizontal span of fixed length at position  $Y$  on the  $y$  axis, the nonlocal correlation function for two strings at  $y=Y_1$  and  $y=Y_2$ , which is given by

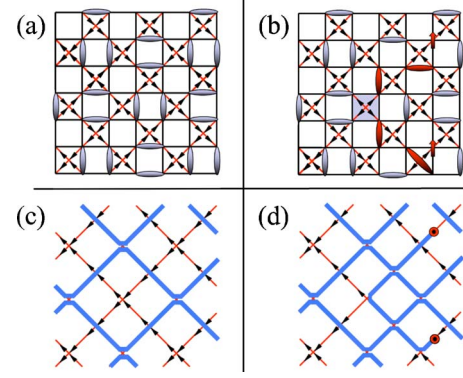


FIG. 6. (Color online) Example of spinon propagation. The potential energy does not depend on the length of the string connecting the pair of spinons, which consequently are in a deconfined phase. In the line representation, the position of each spinon is indicated with a small dotted circle. The shaded square corresponds to a plaquette without singlets that we denote as a defect.

$$\bar{G}(Y_1, Y_2) \equiv \langle e^{i\phi(n_{Y_1} - n_{Y_2})} \rangle, \quad (16)$$

with  $\phi$  arbitrary, is maximal:  $\bar{G}(Y_1, Y_2)=1$ . Because in general  $|G| \leq 1$ , for unrestricted values of  $n_{Y_1}$  and  $n_{Y_2}$ , here one simply has  $n_{Y_1}=n_{Y_2}$ . Similar results apply for the pyrochlore lattice, where  $n_{Y_i}$  denotes the number of lines intersecting the plane  $Y=Y_i$ . Equation (16) presents a high-dimensional analog of the well-known fixed value of string correlation functions in  $S=1$  spin chains at the Affleck-Kennedy-Lieb-Tasaki point.<sup>49,50</sup> At large separations, these uniform nonlocal correlations dwarf the local dimer-dimer correlations, which retain an algebraic decay (as  $r^{-d}$ ). As a direct consequence (below), the system exhibits, in general, a long-ranged dimer order away from the Klein critical point.

#### D. Low-energy excitations at the Klein point: Spinons

The energy cost of exciting one of the singlets of a given dimer configuration is proportional to  $J$ ; as depicted in Fig. 6, this energy is not altered by changes in the separation of the two  $S=1/2$  objects forming the triplet state, which may, thus, be regarded as two deconfined spinon excitations. Single-spinon propagation can be described as a constrained random walk because the allowed paths may not increase the number of tetrahedra without a singlet dimer, but in contrast to the situation in Ref. 7, the paths are far less constrained.

In this context, it is instructive to consider the dimensionality of the allowed spinon paths for the checkerboard and pyrochlore Klein models to examine its relation to the dimensionality  $d_g$  of the symmetry group emerging in the ground state sector.<sup>6</sup> Here,  $d_g$  is the spatial dimensionality of the minimal nonempty set of spins which is influenced by these symmetry operations. Assuming that the ground-state sector does not transform trivially under these symmetry operations, the entropy  $S_g$  scales according to  $S_g \sim N^{d_s/d}$ , where  $d_s=d-d_g$ . The Klein model on the pyrochlore lattice exhibits a zero-dimensional ( $d_g=0$ ) symmetry, meaning that there exist local operations which link different ground states (e.g., the operation depicted in Fig. 4).

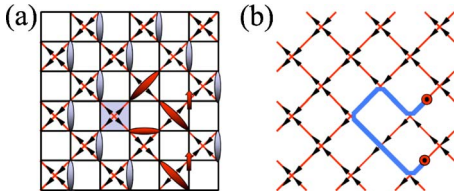


FIG. 7. (Color online) Spinon propagation in the ferroelectric or uniform state depicted in Fig. 5. Disruption of the dimer background dictates that the line or string created between the propagating spinons can move only in the direction indicated by the black arrows. This implies that the spinons are restricted to move within a cone defined by the horizontal and vertical directions. In the line representation, the position of each spinon is indicated with a small dotted circle.

The presence of these symmetries enables spinon excitations to propagate with no energy cost in  $d_s$  dimensions. Thus, spinons on the pyrochlore and checkerboard lattices propagate freely in regions whose size scales with the volume of the entire lattice,  $d_s=d$ . For the square-lattice model of Ref. 7,  $d=2$  while  $d_g=1$ , as a consequence of which the spinons can propagate only in  $d_s=d-d_g=1$  dimensional regions (lines). This analysis provides a more explicit definition of the terms “complete” (pyrochlore and checkerboard) and “partial dimensional reduction” (square lattice) of their origin in terms of system entropy (scaling, respectively, with the volume and with the perimeter) and of their consequences for spinon dynamics.

As noted earlier, perturbation-theoretic calculations, including those illustrating the effects of spinons, are somewhat involved in the dimer basis due to the nonorthogonality of the dimer states. In the remainder of this section, we comment only briefly and qualitatively on possible spinon exchange paths connecting different dimer states of the low-energy sector; a detailed discussion of one systematic approach to quantitative calculations in the dimer basis is deferred to Sec. V.

While we have used the words “free propagation” of spinons to indicate that their motion occurs in all spatial dimensions, spinon dynamics on the pyrochlore and checkerboard lattices at the Klein point remain constrained by the effective ice rules obeyed by the dimer configurations in the ground-state manifold. These rules, upon which we remark further below, become most evident by considering the line representation of the six-vertex model (Fig. 3). In the presence of a single dimer excitation, the allowed lines specify the possible spinon motion. Against the background of the uniform ferroelectric state (corresponding to the line vacuum, Fig. 5), where all horizontal and vertical arrows in the same directions, the spinon lines which may be inserted are all chiral. The spinons are restricted to propagate only within a cone defined by two spatial quadrants (Fig. 7), and no closed spinon paths are possible in such states. The same is true for the opposing ferroelectric state, the state full of lines, in which the string created between the two spinons appears as an antiline.

As suggested by the simple example of the previous paragraph, the spinon motion can be determined from the line rules. The trace left by two spinons, which are created on a

common tetrahedron and move away from each other corresponds, in the line representation, to a string, which changes the state of the underlying link: the string creates a line segment if the link was empty and annihilates the corresponding segment if it were already present. Following the rules of Fig. 3, if the line segment created by the string crosses a pre-existing line, the resulting state on the corresponding tetrahedron is that indicated as 2 in Fig. 3. Once again, we show for clarity in Figs. 6(c) and 6(d) the line representations of the dimer and/or spinon states depicted in Figs. 6(a) and 6(b) for the checkerboard lattice. In the general case of non-uniform states with a finite density of lines, the spinon strings are no longer constrained to be chiral (Fig. 6). When the string of a propagating spinon collides with a six-vertex line representing the dimer configuration, the lines (and hence the spinon path) are effectively reflected.

#### IV. THERMALLY DRIVEN DECONFINEMENT AWAY FROM THE KLEIN POINT

As noted above, the dipolar correlations characterizing the deconfined Klein critical point are driven by classical fluctuations, from where the most appropriate designation is as a classical  $T=0^+$  critical point. Away from  $T=0$ , the critical thermal fluctuations of the dimer coverings produce an entropic spinon-spinon interaction. This interaction may be determined by replacing each spinon with a static monomer inserted in the dimer covering, reducing the problem to the classical statistical mechanics of close-packed dimer coverings.<sup>51,52</sup> This reduction makes use of the fact that the singlet coverings are linearly independent.<sup>53</sup> The critical dipolar fluctuations of the underlying dimer field produce an effective “Coulomb” interaction between the spinons,<sup>17</sup> which, in the pyrochlore lattices under consideration, arises from the local conservation law of zero divergence.

We will demonstrate the existence of the Coulomb phase for the checkerboard lattice; a similar analysis may be applied for the 3D pyrochlore case. The derivation of the effective Coulomb interaction begins by assigning a charge to each spinon, for which it is convenient to expand the six-vertex representation in order to include states containing two spinons. It is important to note that spinons are created in pairs (singlet-triplet excitation), and each pair generates a single crossed plaquette of higher energy, because it possesses no singlets, which will be called a defect. When the spinons propagate away from each other, they are also separated from the defect (Fig. 6), and the preservation of the ice rules requires that the number of defects does not increase. We will show below that the effective charge  $q_d$  of the defect is opposite in sign to the effective charge  $q_s$  of the spinons, with magnitude  $q_d=-2q_s$ . [Superficially, this overall neutrality of three quasiparticles forms a geometric analog of the quark content of the neutron, whose basic quark structure is  $|udd\rangle$  with the charges of the  $u$  and  $d$  quarks being, respectively,  $(2e/3)$  and  $(-e/3)$ .]

To represent states with two spinons, we will include the four additional vertex configurations depicted in Fig. 8. Note that these configurations have nonzero divergence, in contrast to the six-vertex states (Fig. 3) used to represent the

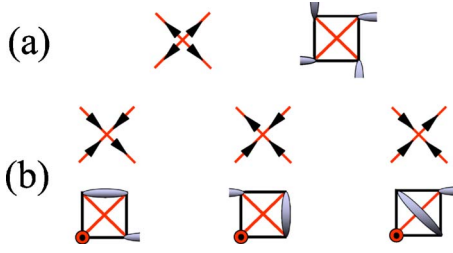


FIG. 8. (Color online) (a) Vertex representation of a crossed plaquette without any singlet (defect). (b) Vertex representation for spinons that are located in one sublattice of the checkerboard lattice.

dimer coverings (which are the vacuum of charge). According to the previous rules, the defect is represented by four outgoing arrows [Fig. 8(a)]. For the checkerboard geometry, it is convenient to introduce the two Néel sublattices  $A$  and  $B$  of the underlying square lattice; a number of equivalent definitions may be found for a two-sublattice decomposition of the 3D pyrochlore. A one-to-one mapping between states containing spinons and the vertex configurations may be found by restricting the spinons to one of the sublattices (for example,  $A$ ). A complete classification of all spinon configurations may be obtained by introducing an additional Ising-like quantum number, which specifies on which of the two sublattices our plaquettes are located. Such an additional tabulation is not necessary for the examination of the long-distance interaction. We may rely instead only on the consequences of the vertex representation illustrated in Fig. 8 for plaquettes of one sublattice, which are sufficient for determining the asymptotic (long-distance) form of the interspinon interaction. The fact that spinons may propagate from one sublattice to the other due to the existence of diagonal bonds in dimer coverings of the checkerboard lattice is, nevertheless, crucial. This is not the case for quantum dimer models on bipartite lattices, whose dimers always link the two different sublattices. We remind the reader that on a bipartite lattice, each spinon may be assigned a unique effective charge given by the sublattice parity of the spinon location (usually  $+1$  on one sublattice, and  $-1$  on the other). This simple assignment is invalid on nonbipartite lattices such as the pyrochlore, where the additional range of possible spinon configurations necessitates an essential extension of the definition of the effective spinon charge.

Because the spinons occupy sites of the original lattice, their position will be denoted by one arrow on the dual lattice. Specifically, we take this as the ingoing arrow coming from the lower left corner of a plaquette with only one outgoing arrow [Fig. 8(b)]. If one considers vertex states such that for each vertex with maximal divergence [Fig. 8(a)] there are two with only one outgoing arrow [Fig. 8(b)], the mapping between the two representations is one to one (under the condition that all the spinons occupy the same sublattice). The Coulomb interaction and the effective charge of the spinons emerge from the standard procedure used to map the ice problem onto a compact  $U(1)$  gauge theory.<sup>54</sup> Here, we follow the derivation and notation of Ref. 55 to describe this procedure and derive the effective charges of defects and spinons.

The local zero-divergence condition defining the dimer coverings on the checkerboard and pyrochlore lattices implies that these states can be considered as the physical Hilbert space of a compact  $U(1)$  gauge theory. The local  $U(1)$  gauge invariance becomes more explicit if one defines pseudospin-1/2 operators  $S_i^z$  on each site  $i$  of the lattice. The dual lattice formed by the centers of the tetrahedrons (vertices) can be divided into two sublattices  $\mathcal{A}$  and  $\mathcal{B}$ . The site coordinate  $i$  of the original lattice denotes the links of the dual lattice.  $S_i^z = 1/2$  if the arrow on link  $i$  points from the  $\mathcal{A}$  to the  $\mathcal{B}$  sublattice, and  $S_i^z = -1/2$  if the arrow points from  $\mathcal{B}$  to  $\mathcal{A}$ . The zero-divergence condition can be expressed in terms of these variables as

$$\sum_{i \in \mathcal{A}} S_i^z = 0, \quad (17)$$

and the operators

$$U_\alpha = e^{i\phi_\alpha \sum_{i \in \mathcal{A}} S_i^z} \quad (18)$$

are the local  $U(1)$  symmetry transformations associated with this conservation law. We note that the conservation law is a property of the Hilbert space and is, therefore, present for any theory defined on this space. An equivalent constrained low-energy Hilbert space was derived for an XXZ model on a pyrochlore lattice in Ref. 20.

We present in some detail the consequences of the zero-divergence condition for the checkerboard lattice ( $d=2$ ), for which the notation is slightly more compact; the results we obtain are unchanged for the pyrochlore lattice ( $d=3$ ). The  $U(1)$  gauge structure of the Hilbert space indicates that one may gain further insight by identifying the variables playing the role of the electric field and of the vector potential in electrodynamics. For this purpose, it is convenient to introduce quantum rotor variables and the coordinate  $\mathbf{r} = n\mathbf{e}_1 + m\mathbf{e}_2$  to span the dual lattice (the lattice of centers of the tetrahedrons). The primitive vectors  $\mathbf{e}_1$  and  $\mathbf{e}_2$  define the two perpendicular directions on the dual lattice. On each link of this lattice, we define an angular-momentum variable  $\tilde{l}_\mu(\mathbf{r}) = \pm 1/2$ , where  $\mu(\mathbf{r})$  indicates the oriented link from  $\mathbf{r}$  to a neighboring dual-lattice site  $\mathbf{r} + \mathbf{e}_\mu$ . The state  $\tilde{l}_\mu(\mathbf{r}) = 1/2$  [ $\tilde{l}_\mu(\mathbf{r}) = -1/2$ ] corresponds to an arrow parallel (antiparallel) to the relative vector  $\mathbf{e}_\mu$ . With this definition,  $\tilde{l}_\mu(\mathbf{r})$  changes sign under inversion:  $\tilde{l}_{-\mu}(\mathbf{r}) = -\tilde{l}_\mu(\mathbf{r})$  [ $-\mu(\mathbf{r})$  indicates the oriented link from  $\mathbf{r}$  to  $\mathbf{r} - \mathbf{e}_\mu$ ]. For convenience, we introduce the variable  $l_\mu(\mathbf{r}) = \tilde{l}_\mu(\mathbf{r}) + 1/2$ , which takes the integer values 0 or 1. We employ the discrete gradient

$$\nabla_\mu l_\nu(\mathbf{r}) = l_\nu(\mathbf{r}) - l_\nu(\mathbf{r} - \mathbf{e}_\mu) \quad (19)$$

to re-express the ice rules as an explicit zero-divergence condition on the vector field  $l_\mu(\mathbf{r})$  as follows:

$$\sum_{\mu=1,2} \nabla_\mu l_\mu(\mathbf{r}) = 0. \quad (20)$$

Equation (20) corresponds to Gauss's law for electrodynamics in the absence of external charges,  $\nabla \cdot \mathbf{E} = 0$ . The vertex configurations violating the ice rules, such as those depicted

in Fig. 8, should then carry an “effective charge”  $Q = \sum_{\mu=1,2} \nabla_{\mu} l_{\mu}(\mathbf{r})$ . Here,  $Q = \sum_{\mu=1,2} \nabla_{\mu} l_{\mu}(\mathbf{r}) = 2$  for the configurations of Fig. 8(a) (defects) and  $Q = \sum_{\mu=1,2} \nabla_{\mu} l_{\mu}(\mathbf{r}) = -1$  for the three configurations of Fig. 8(b) (spinons): the spinons carry a positive unit charge while the defects carry two units of negative charge. The “electric field” is then defined as the operator  $\mathbf{E}_{\mu}(\mathbf{r})$  with eigenstates  $|l_{\mu}(\mathbf{r})\rangle$  and eigenvalues  $l_{\mu}(\mathbf{r})$ . The canonically conjugate operator  $\Theta_{\nu}(\mathbf{r})$  satisfying

$$[\Theta_{\nu}(\mathbf{r}'), \mathbf{E}_{\mu}(\mathbf{r})] = i \delta_{\mathbf{r},\mathbf{r}'} \delta_{\mu,\nu} \quad (21)$$

plays the role of the vector potential. Because in this section we focus only on the high-temperature ( $T \rightarrow \infty$ ) fixed point whose properties are determined solely by the gauge structure of the Hilbert space, we will not discuss any particular quantum gauge theory. The above derivation is used only to identify which variables play the role of the electric field and the charge.

The Klein point at  $T=0^+$  corresponds to the infinite-temperature fixed point. Such a point is characterized by a deconfined two-component (spinons and defects) Coulomb gas. The spinons exist only as gapped excitations (of gap  $\Delta \propto J$ ), and the spinon-spinon interaction is then logarithmic,  $V(r) = \gamma \sum_{j < k} q_j q_k \ln(r_{jk}/a)$ , for  $d=2$  and a power law,  $V(r) = \tilde{\gamma} \sum_{j < k} q_j q_k / r_{jk}^d$ , for  $d=3$ . The spinon-defect interaction has the opposite sign (attractive) and its absolute value is two times greater. Although a spinon-defect pair is critically confined in the  $d=2$  case by the logarithmic interaction, the prefactor  $\gamma$  is generally sufficiently small that there is a divergence in the expectation value of  $\langle r^2 \rangle$ , which implies a divergent “dielectric constant.”<sup>56</sup> At finite temperatures, there is a finite concentration  $\rho \sim e^{-\beta \Delta}$  [ $\beta = (k_B T)^{-1}$ ] of thermally excited spinons in equilibrium, and the effective spinon-spinon or spinon-defect interaction is screened, decaying exponentially for distances  $r \gg 1/\rho^{1/d}$ . However, the critical behavior remains observable for  $r \ll 1/\rho^{1/d}$ .

For general  $K \neq K_c$  and  $|K - K_c| \ll J$ , the energy difference between the singlet and triplet states on each tetrahedron is much smaller than the gap to the quintet state ( $S=2$ ).<sup>57</sup> It is clear that for  $\epsilon = |K - K_c| \ll J$ , the degeneracy between the singlet and triplet states is effectively restored at temperatures  $T$  such that

$$\epsilon \ll k_B T \ll J. \quad (22)$$

In this case, only the manifold of singlet dimer coverings found as the ground states at  $K=K_c$  is accessible. Thus, the effect of a finite temperature on a system in the proximity of a Klein point is the effective restoration of extensive configurational entropy, critical dipolar correlations, topological order, and spinon deconfinement.

We comment that the appearance of deconfinement at high temperatures, also in systems far more general than those considered here, is hardly surprising. We repeat the well-known facts as follows: various ordered phases generally melt via the appearance of topological defects; these defects become deconfined at the melting temperature; the origin of deconfinement is an energy-entropy balance; and entropic effects modify the effective interactions between the

defects, leading to a vanishing interaction at the onset of deconfinement. A careful treatment of entropic effects often involves detailed contour-counting arguments.<sup>58</sup> The effective force between topological defects in a wide range of systems, including vortices in superconductors and dislocations and disclinations in elastic media, is universally expected to be algebraic, as may be seen directly from duality arguments.<sup>59–61</sup> In the current context, the topological defects correspond to monomers or spinons in the dimer coverings and the Coulomb field lines to the many possible trajectories for the motion of a defect. Pure Coulomb interactions vanish at large separations in dimensions  $d > 2$ , suggesting the possibility of a high-dimensional fractionalization. The peculiar aspect of the pyrochlore systems under consideration is that the critical point separating the low-temperature confined state from the high-temperature deconfined phase may be driven to  $T=0^+$  by optimizing the frustration in  $H$ . This is the singular characteristic of the Klein point: the exponentially large ground-state sector is defined solely by the local zero-divergence constraint. The system is then driven only by entropic fluctuations, which in combination with the local constraint give rise to the classical critical behavior.

## V. ZERO-TEMPERATURE STATES AWAY FROM THE KLEIN POINT

### A. Local perturbations in the nonorthogonal dimer basis

In this section, we explicitly examine the possible ground states away from the Klein point. To this end, we begin by developing a systematic procedure for evaluating “matrix elements”  $\langle \psi_a | \hat{O} | \psi_b \rangle$  within the nonorthogonal basis of singlet dimer coverings, which constitute the low-energy sector in the vicinity of the Klein point. We note that because of the nonorthogonality, a standard (bra-operator-ket) expectation value computed between two states in the manifold is not a true matrix element, and is referred to henceforth as a “bracket.” We will illustrate the calculational procedure and the results for the checkerboard lattice, and state only that their generalization to the pyrochlore is straightforward (if lengthy).

The evaluation procedure consists of elementary rules, which are applied to the graph associated with the bracket to be evaluated, and it is a generalization of the standard method used to compute the overlap between two singlet dimer coverings on bipartite lattices.<sup>62–65</sup> We first extend this method to compute the overlap between nonbipartite singlet coverings, because on the pyrochlore system the dimers are not necessarily formed from sites on different sublattices. Second and more importantly, we provide straightforward rules for computing brackets of spin-product operators of Heisenberg type,  $\vec{S}_i \cdot \vec{S}_j$ . Brackets of products of Heisenberg spin operators, as in the second term of Eq. (1), can be evaluated by a simple extension of these rules.

In this section, we will consider a perturbation, which is proportional to the first term of Eq. (1), a Heisenberg interaction between any pair of sites in the same crossed plaquette,

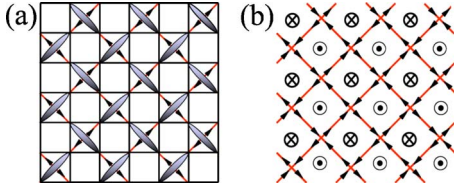


FIG. 9. (Color online) The “antiferroelectric” state. Dots and crosses at the centers of the plaquettes of the dual lattice indicate the “flux” associated with the arrow circulation on the corresponding plaquette. The two antiferroelectric states are the only ones for which each plaquette of the dual lattice has a net chirality.

$$H_1 = \Delta J \sum_{\langle ij \rangle, \alpha} \vec{S}_i^\alpha \cdot \vec{S}_j^\alpha, \quad (23)$$

such that after the perturbation  $K \neq 4J/5$ . For the Klein model on the square lattice, it is transparent that all states within the ground-state basis remain degenerate to first order in the perturbation  $H_1$ . This statement follows from two observations: the diagonal brackets,  $\langle \psi_a | H_1 | \psi_a \rangle$ , are the same for any dimer state  $|\psi_a\rangle$  and the off-diagonal terms,  $\langle \psi_a | \hat{O} | \psi_b \rangle$ , with  $a \neq b$ , are zero for any local operator  $\hat{O}$ , in particular, for  $\hat{O} = H_1$ . Thus, the degeneracy is lifted only to the second order in  $H_1$  on the square lattice. The situation is completely different for the same model on the pyrochlore and checkerboard lattices: because in these cases the ground-state degeneracy is extensive at the Klein point, two different ground states can be connected by local operators. As a consequence, the off-diagonal brackets do not, in general, vanish, and the degeneracy is lifted to the first order in the perturbation.

The usual approach to this problem is to neglect the non-orthogonality of the singlet dimer coverings and propose a minimal quantum dimer model, which includes only processes of the Rokhsar-Kivelson (RK) type.<sup>64</sup> We note, however, that this procedure does not lead to the RK model in the pyrochlore geometries under consideration because, although the Hamiltonian is the same [a  $U(1)$  gauge magnet<sup>66</sup>], the zero divergence or gauge condition which defines the “physical” Hilbert spaces is different. In what follows, we depart from this conventional treatment and show that it is indeed incorrect for the case of interest. The nonorthogonality of the dimer basis introduces subtleties not directly evident from the conventional approach, as a consequence of which we will show that the valence-bond crystal (VBC) orderings chosen by tunneling events differ from the ones expected for a theory which includes only processes of the RK type.<sup>67</sup>

In terms of the arrows (of the six-vertex representation of Fig. 2) shown in Fig. 9, the antiferroelectric state becomes a staggered flux phase in which each square plaquette of the dual lattice has a well-defined chirality (all of its arrows circulate in the same way) and the direction of circulation alternates from clockwise to counterclockwise. With this starting state, one may invert the sign of the current (direction of the arrows) around any plaquette. This is the elementary process, or corner flip in the line representation, depicted in Fig. 4(b). The antiferroelectric state allows for the largest number

of these elementary processes, and each can be interpreted as the creation of a localized defect on an uncrossed plaquette of the antiferroelectric background. The tunneling between states with defects in different positions lowers the energy of the system. While the creation of one of these defects is indeed the elementary RK process normally invoked as the most relevant one in these cases,<sup>39</sup> we will show that its amplitude is exactly equal to zero for the perturbation  $H_1$ .

To first order in the perturbation, the state of lowest energy is the linear combination of singlet dimer coverings, which minimizes  $H_1$ . Up to an irrelevant constant, the Hamiltonian  $H_1$  can be rewritten in the more convenient form as follows:

$$H_1 = \frac{1}{2} \Delta J \sum_{\langle ij \rangle, \alpha} P_{ij}^\alpha, \quad (24)$$

where  $P_{ij}^\alpha$  is the permutation operator, which interchanges the spins on sites  $i$  and  $j$  of plaquette  $\alpha$ . The diagonal brackets are manifestly the same for all singlet dimer coverings. Specifically, on the checkerboard lattice and for any system with PBCs,

$$E_d = \langle \psi_a | H_1 | \psi_a \rangle = \frac{3}{8} N \Delta J, \quad (25)$$

with  $N$  the number of lattice sites and  $|\psi_a\rangle$  denoting any dimer covering satisfying the Klein constraint (all crossed plaquettes contain one dimer). As noted in Sec. III, the systems with OBCs possess additional ground states containing crossed plaquettes with two dimers or (one or two) spinons, and these would have a different diagonal energy but are not thermodynamically relevant. We focus henceforth on ground states satisfying PBCs. The degeneracy of dimer coverings is lifted only by superposing different allowed coverings with finite amplitudes, i.e., by considering states of the form

$$|\psi\rangle = \sum_a c_a |\psi_a\rangle, \quad (26)$$

with the normalization condition

$$\sum_k |c_k|^2 + \sum_{l \neq k} c_l^* c_k \langle \psi_l | \psi_k \rangle = 1. \quad (27)$$

## B. Loop structure and rules

We proceed by listing a complete set of rules for the evaluation of brackets in the dimer basis. These general, purely topological, rules extend early and pioneering ideas concerning resonating valence-bond states and initial results obtained by using these concepts for square lattices.<sup>62–65</sup> The normalization of  $|\psi\rangle$  and computation of  $\langle \psi | H_1 | \psi \rangle$  require evaluating the overlaps  $\langle \psi_a | \psi_b \rangle$  and brackets of the form  $\langle \psi_a | P_{ij} | \psi_b \rangle$ , with  $|\psi_a\rangle$  and  $|\psi_b\rangle$  any states in the dimer basis. To compute the overlap, we first assign a given orientation to each singlet dimer, indicated with arrows pointing upwards for vertical dimers and to the right for diagonal and horizontal bonds (Fig. 10). (We remark that vertical and horizontal refer here to the real lattice and not to the rotated lattice used in the discussion of the six-vertex and line representations in Sec. III.) With this convention, a superposition of dimer con-

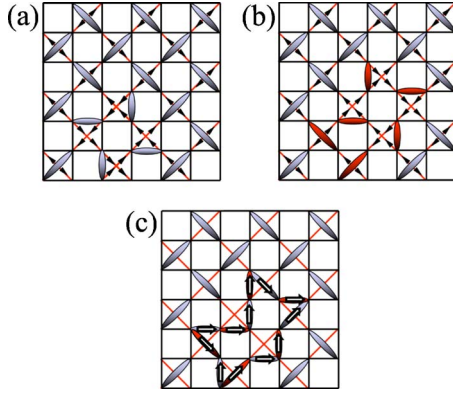


FIG. 10. (Color online) Example (c) of the graph  $G^{ab}$  which results from superposing two different dimer coverings [(a) and (b)]. These dimer coverings correspond to an antiferroelectric background with a single elementary process operating on different (nearest-neighbor) uncrossed plaquettes.

figurations corresponding to  $|\psi_a\rangle$  and  $|\psi_b\rangle$ , with the differing bonds marked as in Fig. 10(c) (bonds which do not differ give trivial loops of length 2, introducing factors of unity), forms a graph  $G^{ab}$ . In general, this graph may consist of more than one disconnected loop  $\Gamma_j^{ab}$ .

Let  $L(\Gamma_j^{ab})$  be the length of the loop  $\Gamma_j^{ab}$  (the number of singlet dimers forming the loop),  $N_\Gamma(G^{ab})$  be the number of disconnected loops in graph  $G^{ab}$ , and  $n_c$  be the number of arrows in the graph, which circulate clockwise in their loop. With these definitions, the overlap  $\langle\psi_a|\psi_b\rangle$  may be expressed as

$$g_{ab} = \langle\psi_a|\psi_b\rangle = (-1)^{n_c + L(G^{ab})/2} 2^{N_\Gamma(G^{ab}) - L(G^{ab})/2}, \quad (28)$$

where

$$L(G^{ab}) = \sum_{j=1, N_\Gamma(G^{ab})} L(\Gamma_j^{ab}) \quad (29)$$

is the total length of the graph. The determination of the nontrivial brackets  $\langle\psi_a|P_{ij}|\psi_b\rangle$  proceeds by examining how the length and dimer orientation of the graph  $G^{ab}$  are affected when the permutation operator  $P_{ij}$  is applied to the state  $|\psi_b\rangle$ . The resulting graph will be denoted as  $G_{ij}^{ab}$ . The application of  $P_{ij}$  may alter the loop geometry in only a restricted set of simple ways, of which we next provide a systematic list.

(i) If  $i, j \in G^{ab}$  and they belong to the same loop  $\Gamma$ , there are two possibilities.

(a) When the distance (number of dimers) on the loop between sites  $i$  and  $j$  is an odd number, the effect of  $P_{ij}$  is to cut the loop into two segments and to reconnect them while exchanging the ends of one of the segments [Figs. 11(a) and 11(b)]. The length of the loop under consideration is unaltered in this process. The only effective modification is the reversal of an odd number of arrows, causing a sign-change relative to  $\langle\psi_a|\psi_b\rangle$ ,

$$\langle\psi_a|P_{ij}|\psi_b\rangle = -g_{ab}. \quad (30)$$

(b) When the distance between sites  $i$  and  $j$  is even,

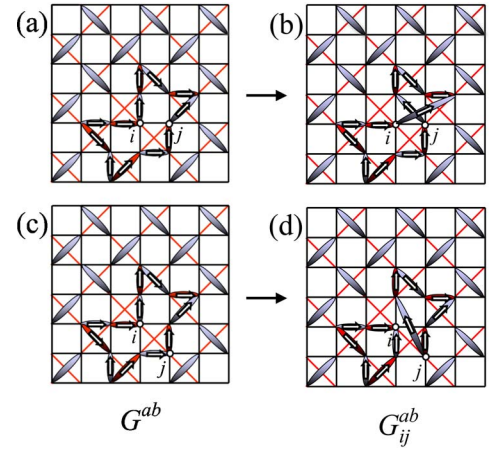


FIG. 11. (Color online) Effect of the permutation operator  $P_{ij}$  on graph  $G^{ab}$  (Fig. 10) when sites  $i$  and  $j$  belong to the same loop of  $G^{ab}$  and their separation is odd [case (a)  $\rightarrow$  (b)] or even [case (c)  $\rightarrow$  (d)].

$P_{ij}$  divides the loop  $\Gamma$  into two smaller loops,  $\Gamma_1$  and  $\Gamma_2$ , preserving the total length,  $L(\Gamma) = L(\Gamma_1) + L(\Gamma_2)$  [Figs. 11(c) and 11(d)]. The circulation of the arrows is unaltered, and thus from Eq. (28) the net change relative to graph  $G^{ab}$  is a supplementary factor of 2 due to the increase in the number of loops,  $N_\Gamma(G_{ij}^{ab}) = N_\Gamma(G^{ab}) + 1$ , where

$$\langle\psi_a|P_{ij}|\psi_b\rangle = 2g_{ab}. \quad (31)$$

(ii) If only one of the two sites ( $i$  or  $j$ ) belongs to graph  $G^{ab}$ , the effect of  $P_{ij}$  is to increase the length of the graph by two links,  $L(G_{ij}^{ab}) = L(G^{ab}) + 2$ . There is no change of sign because the arrows of the two additional bonds circulate in opposite directions relative to their point of contact. From Eq. (28), the net result relative to graph  $G^{ab}$  is a factor of  $1/2$  due to the length increase, and so

$$\langle\psi_a|P_{ij}|\psi_b\rangle = \frac{1}{2}g_{ab}. \quad (32)$$

(iii) If neither  $i$  nor  $j$  belongs to graph  $G^{ab}$ , there are two possible cases.

(a) If there is a singlet bond connecting the sites  $i$  and  $j$ ,

$$\langle\psi_a|P_{ij}|\psi_b\rangle = -g_{ab}. \quad (33)$$

(b) If the sites  $i$  and  $j$  are not connected by a singlet bond,

$$\langle\psi_a|P_{ij}|\psi_b\rangle = \frac{1}{2}g_{ab}. \quad (34)$$

(iv) Finally, if  $i, j \in G^{ab}$  but the sites belong to different loops  $\Gamma_i$  and  $\Gamma_j$ , the effect of  $P_{ij}$  is to fuse both loops into a single loop  $\Gamma_{ij}$ . Because the total length,  $L(\Gamma_{ij}) = L(\Gamma_i) + L(\Gamma_j)$ , and the sign are preserved under this operation, the net result is a factor of  $1/2$  which arises from the decrease by one in the number of loops,  $N_\Gamma(G_{ij}^{ab}) = N_\Gamma(G^{ab}) - 1$ , leading to

$$\langle\psi_a|P_{ij}|\psi_b\rangle = \frac{1}{2}g_{ab}. \quad (35)$$

These rules allow a very straightforward derivation of Eq. (25): because  $G^{aa}$  is the null graph, the effect of  $P_{ij}$  corresponds to case (iii). For any dimer covering, there are  $N/2$  bonds of type (iii)(a) and  $5N/2$  bonds of type (iii)(b) and adding the two contributions yields

$$E_d = \langle \psi_a | H_1 | \psi_a \rangle = \frac{1}{2} \Delta J \left( -g_{aa} \frac{N}{2} + \frac{g_{aa} 5N}{2} \right). \quad (36)$$

From  $g_{aa} = 1$  [see Eq. (28)], we recover Eq. (25).

With the same rules, one may compute the energy of the most general state within the Klein-point ground-state manifold whose expression is given by Eq. (26),

$$E = E_d + \frac{1}{2} \Delta J \sum_{l \neq k} c_l^* c_k \left[ g_{lk} \left( \frac{3L(G^{lk})}{4} - \frac{|\mathcal{V}^{lk}|}{2} \right) + W_{lk} \right]. \quad (37)$$

Here,  $W_{lk} \equiv 2n_{ib}^{lk} - n_{ia}^{lk}$ , where  $n_{ia}^{lk}$  ( $n_{ib}^{lk}$ ) is the number of pairs  $\langle i, j \rangle$  which are of type (i)(a) ((i)(b)) relative to the graph  $G^{lk}$ , while  $\mathcal{V}^{lk} = n_{ia}^{lk} + n_{ib}^{lk}$  is the total number of pairs  $\langle i, j \rangle$  of type (i). The reason why only cases of type (i) need be considered in Eq. (37) is that terms of types (ii), (iii)(b), and (iv) all give the same contribution,  $g_{ab}/2$ .

### C. Energy calculations

Next, we apply the rules of Sec. V B to the checkerboard lattice. Equation (37) allows one to compute the energy of any variational state. Its second term corresponds to the energy change  $\delta E$  due to the linear combination of different singlet dimer coverings. The magnitude of this change therefore reflects the degree of ‘‘mixing’’ between different dimer coverings induced by  $H_1$ . To develop an intuitive understanding, we begin by considering the linear combination of two dimer coverings, a natural choice being to superpose two coverings whose dimer configurations differ minimally (such as the two states depicted in Fig. 4), i.e., by the RK or corner-flip process discussed above. We remind the reader that the six-vertex representation of this process entails a reversal of the arrows on a single plaquette of the dual lattice with a well-defined chirality [Figs. 12(a) and 12(b)]. If  $|\psi_o\rangle$  and  $|\psi_d\rangle$  are any such pair of dimer coverings which differ minimally, their overlap is

$$g_{od} = \langle \psi_o | \psi_d \rangle = 2 \times 2^{-4} = \frac{1}{8}, \quad (38)$$

because  $L(G^{od}) = 8$  and  $n_c = 4$  [Fig. 12(c)]. To obtain the energy of the normalized state

$$|\psi_{od}\rangle = \alpha |\psi_o\rangle + \beta |\psi_d\rangle, \quad (39)$$

one replaces the coefficients of Eq. (37) with the values dictated by the above rules. The number of pairs  $\langle i, j \rangle$  with both sites on the graph is  $|\mathcal{V}^{od}| = 12$ , which is composed of eight pairs of type (i)(a) and four of type (i)(b) as a result of which  $W^{od} = 0$ . Replacing these quantities in Eq. (37) gives

$$\langle \psi_{od} | H_1 | \psi_{od} \rangle = E_d. \quad (40)$$

The fact that the energy is unchanged ( $\delta E = 0$ ) by taking the linear combination (39) indicates that the elementary RK-

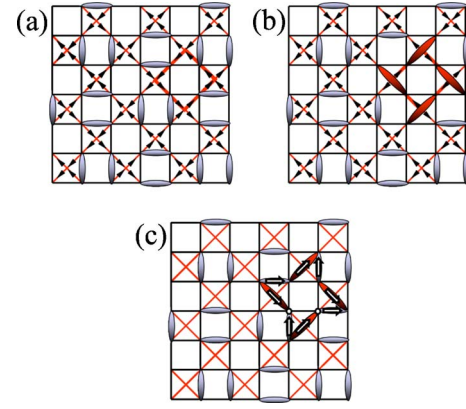


FIG. 12. (Color online) Graph  $G^{od}$  resulting from the superposition of two dimer coverings, which differ minimally. The physical process connecting these is the RK-type or corner-flip process represented in Fig. 4.

type process is not generated by  $H_1$ . We note that all pairs of sites  $\langle i, j \rangle$  in the only loop of the graph  $G^{od}$  [Fig. 12(c)] are separated by a distance on the loop no greater than 2; loops satisfying this condition will be defined as *simple*. As an example, the loop depicted in Fig. 10(c) is not simple because it contains site pairs  $\langle i, j \rangle$  separated by five and six bonds. In general,  $\delta E$  vanishes for any pair of dimer configurations,  $|\psi_a\rangle$  and  $|\psi_b\rangle$ , such that all loops in the graph  $G^{ab}$  are simple. This property follows immediately from Eq. (37): if all loops are simple, one has that  $n_{ia}^{ab} = 2n_{ib}^{ab} = L(G^{ab})$ , implying  $W_{ab} = 0$  and  $|\mathcal{V}^{ab}| = 3L(G^{ab})/2$ .

Because  $H_1$  does not connect two minimally different dimer configurations [ $L(G^{ab}) = 8$ ], it is necessary to seek the minimal relevant process, which means that process with the minimum value of  $L(G^{ab})$ , which is generated by  $H_1$ . The next possible value is  $L(G^{ab}) = 12$  [no graphs exist with  $L(G^{ab}) = 10$ ], an example of such a physical process being that connecting the states (a) and (b) in Fig. 10. In the six-vertex representation, this process is permitted when all the arrows of a rectangle formed by two adjacent plaquettes of the dual lattice have the same chirality; this rectangle is highlighted in Figs. 10(a) and 10(b). The process consists of inverting the orientation of the six arrows, or the flux of the rectangle. For any pair of dimer coverings  $|\psi_0\rangle$  and  $|\psi_1\rangle$ , which differ by this process,

$$g_{01} = \langle \psi_0 | \psi_1 \rangle = -2 \times 2^{-6} = -\frac{1}{32}, \quad (41)$$

and for the normalized linear combination  $|\psi_{01}\rangle = c_0 |\psi_0\rangle + c_1 |\psi_1\rangle$  the energy change is

$$\langle \psi_{01} | H_1 | \psi_{01} \rangle = E_d + \frac{3}{64} c_0 c_1 \Delta J. \quad (42)$$

The minimum energy is obtained for  $|c_0| = |c_1|$ , which together with the normalization condition gives  $c_0 = c_1 = 1/\sqrt{2(1+g_{01})}$  for  $\Delta J < 0$  and  $c_0 = -c_1 = 1/\sqrt{2(1-g_{01})}$  for  $\Delta J > 0$ . The overlap is  $|g_{01}| = \frac{1}{32} \ll 1$ , giving  $|c_0| = |c_1| \sim 1/\sqrt{2}$ , as expected for the mixing of two orthogonal states with the same diagonal energy. This remains true for any pair of states connected by  $H_1$  because  $|g_{01}|$  is an upper bound for the absolute value of their overlap.

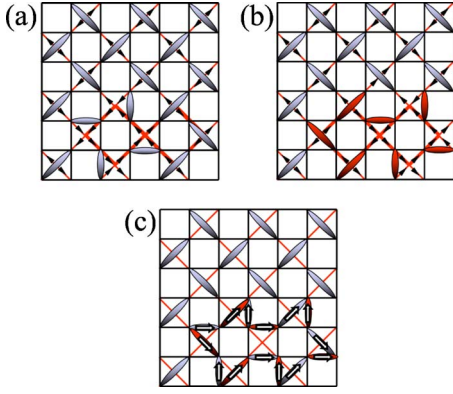


FIG. 13. (Color online) Graph  $G^{ab}$  resulting from the superposition of two states connected by inverting the arrows of two next-neighbor plaquettes of the dual lattice, which have opposing, well-defined chiralities. The two plaquettes are highlighted in panels (a) and (b).

In the next process to consider, the arrow directions on the perimeters of two next-neighbor plaquettes of the dual lattice are inverted if both plaquettes have opposing, well-defined chiralities, as indicated in the examples of Figs. 13(a) and 13(b). In this case, we denote the corresponding dimer coverings by  $|\psi_0\rangle$  and  $|\psi_2\rangle$ , and the length of the associated graph is  $L(G^{02})=14$ . The overlap is  $g_{02}=1/64$  and the energy shift due to the perturbation for the linear combination  $|\psi_{02}\rangle=c_0|\psi_0\rangle+c_2|\psi_2\rangle$  is

$$\langle\psi_{02}|H_1|\psi_{02}\rangle=E_d-\frac{3}{128}c_0c_2\Delta J, \quad (43)$$

with  $c_0=\pm c_2=1/\sqrt{2(1\pm g_{02})}$  for  $\Delta J=\pm|\Delta J|$ .

The other graph  $G^{ab}$  of length  $L(G^{ab})=14$  corresponds to a process, which is analogous to the previous case but with next-neighbor plaquettes of the dual lattice having the same well-defined chirality (Fig. 14). The energy change  $\delta E$  associated with this process is exactly that obtained for  $|\psi_{02}\rangle$ . Any other process generated by  $H_1$  has an associated graph of length  $L(G^{ab})>14$ , and because the amplitude of these

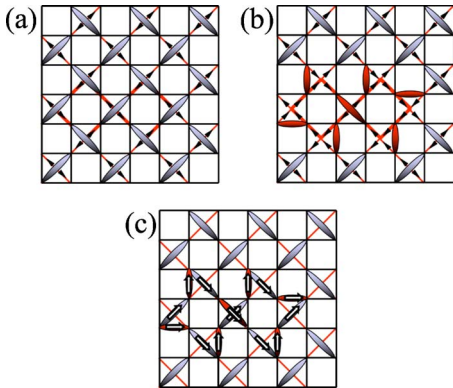


FIG. 14. (Color online) Graph  $G^{ab}$  resulting from the superposition of two states connected by inverting the arrows of two next-neighbor plaquettes of the dual lattice which have the same well-defined chirality. The two plaquettes are highlighted in panels (a) and (b).

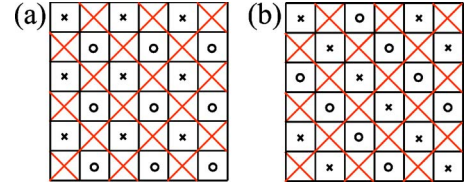


FIG. 15. (Color online) (a) Néel and (b) colinear alternations of uncrossed plaquettes on two sublattices. (a) Decomposition of uncrossed plaquettes of the checkerboard system into two sublattices  $A$  (crosses) and  $B$  (circles), which dictates the form of the variational wave function (44) for  $\Delta J>0$ ; (b) decomposition into sublattices  $C$  (crosses) and  $D$  (circles), which yields the form of the low-energy wave function for  $\Delta J<0$ .

processes falls in proportion to  $n_{ns}^{ab}2^{-L(G^{ab})/2}$  [ $n_{ns}^{ab}$  is the number of pairs  $\langle i,j\rangle$  on the same loop separated by a distance greater than 2], these may safely be cut off beyond a certain length  $L_c(G^{ab})$ .

#### D. Variational wave function

In order to propose a wave function  $|\psi\rangle$ , which takes advantage of the three processes giving nonzero contributions for  $L(G^{ab})\leq 14$ , we introduce the bosonic operators  $\Delta_{\vec{a}}^{\dagger}$  and  $\Delta_{\vec{a}}$ . To define these operators, we classify the uncrossed plaquettes of the checkerboard lattice according to the sublattice  $A$  or  $B$  (Sec. IV) of the dual square lattice [Fig. 15(a)]. In the six-vertex representation of the antiferroelectric state (Fig. 9), these two sublattices have opposite chirality, corresponding to a staggered flux phase. If the uncrossed plaquette  $\vec{a}$  has a well-defined chirality, the operator  $\Delta_{\vec{a}}^{\dagger}$  raises the flux from negative to positive if  $\vec{a}\in A$  and lowers it from positive to negative if  $\vec{a}\in B$ , i.e.,  $\Delta_{\vec{a}}^{\dagger}$  changes the direction of arrow circulation from counterclockwise to clockwise if  $\vec{a}\in A$  and conversely if  $\vec{a}\in B$ . For states of no well-defined chirality on plaquette  $\vec{a}$ , and when the flux is positive (negative) for  $\vec{a}\in A(B)$ ,  $\Delta_{\vec{a}}^{\dagger}$  becomes the null operator,  $\Delta_{\vec{a}}^{\dagger}|\psi_a\rangle=0$ .

Minimizing the energy of a variational state is equivalent to maximizing the number of allowed tunneling processes with a negative sign. The appropriate dimer background for this optimization is provided by the antiferroelectric state  $|\psi_{afe}\rangle$  of Fig. 9; only for this state can the elementary process of Fig. 12 be applied to every uncrossed plaquette. Moreover, the three processes, which give finite contributions to  $\delta E$  for  $L(G^{ab})\leq 14$  can be applied to any pair of nearest-neighbor (Fig. 10) and next-neighbor (Figs. 13 and 14) plaquettes of the dual lattice when the antiferroelectric background is suitably populated with the local defects (bosons) created by  $\Delta_{\vec{a}}^{\dagger}$ . For positive  $\Delta J$ , these processes lead to a uniform energy gain ( $\delta E<0$ ) when the bosons are created with opposite phases on the sublattices  $A$  and  $B$  [Fig. 15(a)]. The considerations for  $\Delta J<0$  mirror those for positive  $\Delta J$  with a change of the decomposition in two sublattices: for negative  $\Delta J$ , the uniform energy gain occurs when the bosons are created with opposite phases on the sublattices  $C$  and  $D$  [Fig. 15(b)]. Employing the definitions and observa-

tions introduced earlier in this section, the simplest wave functions for approximating the ground state in the presence of  $H_1$  are

$$|\psi_+\rangle = u^N \prod_{\bar{\alpha} \in A} (1 + \Delta_{\bar{\alpha}}^\dagger) \prod_{\bar{\alpha} \in B} (1 - \Delta_{\bar{\alpha}}^\dagger) |\psi_{\text{afe}}\rangle,$$

$$|\psi_-\rangle = v^N \prod_{\bar{\alpha} \in C} (1 + \Delta_{\bar{\alpha}}^\dagger) \prod_{\bar{\alpha} \in D} (1 - \Delta_{\bar{\alpha}}^\dagger) |\psi_{\text{afe}}\rangle, \quad (44)$$

where  $|\psi_\pm\rangle$  correspond to  $\Delta J = \pm|\Delta J|$ . The coefficients  $u$  and  $v$  are determined from the normalization of the corresponding wave functions [Eq. (27)]. Figure 15 illustrates the sublattice decompositions of the checkerboard geometry for the two cases:  $(A, B)$  for  $\Delta J > 0$  ( $|\psi_+\rangle$ ) and  $(C, D)$  for  $\Delta J < 0$  ( $|\psi_-\rangle$ ). A similar decomposition into plaquettes  $C'$  and  $D'$  is obtained by a  $\pi/2$  rotation of Fig. 15(b).

The wave functions  $|\psi_+\rangle$  and  $|\psi_-\rangle$  represent linear combinations including all possible two-plaquette resonance processes, the phase relations of which are specified by Fig. 15. Although these are superpositions of many states from the manifold of dimer coverings, the number of participating coverings remains a very small fraction of the total, and the selected linear combinations are VBC states. In the pseudospin  $\tau=1/2$  space generated by the two possible states of each uncrossed plaquette of  $|\psi_{\text{afe}}\rangle$ ,  $|\psi_+\rangle$  and  $|\psi_-\rangle$  are analogous to the classical, magnetically ordered Néel [ $\vec{q}=(\pi, \pi)$ ] and colinear [ $\vec{q}=(0, \pi)$  or  $\vec{q}=(\pi, 0)$ ] states polarized in the  $\hat{x}$  direction. In this space,  $|\psi_{\text{afe}}\rangle$  corresponds to one of the fully polarized ferromagnetic states (such as  $\tau_{\bar{\alpha}}^z = -1/2$  for all  $\bar{\alpha}$ ). However,  $|\psi_+\rangle$  and  $|\psi_-\rangle$  are not exactly the classical Néel and colinear states because two nearest-neighbor uncrossed plaquettes cannot be “flipped” independently of each other, i.e.,

$$\Delta_{\bar{\alpha}}^\dagger \Delta_{\bar{\alpha}'}^\dagger |\psi_{\text{afe}}\rangle = 0 \quad (45)$$

if  $\bar{\alpha}$  and  $\bar{\alpha}'$  are nearest-neighbor uncrossed plaquettes. In the pseudospin representation the two plaquettes cannot be simultaneously in the  $\tau^z=1/2$  state, as a result of which these states are projected out of the superpositions corresponding to the classical Néel and colinear states to obtain  $|\psi_+\rangle$  and  $|\psi_-\rangle$ . We stress that the symmetries of  $|\psi_+\rangle$  and  $|\psi_-\rangle$  for  $\Delta J = \pm|\Delta J|$  are quite different.

The energies of the wave functions  $|\psi_+\rangle$  and  $|\psi_-\rangle$  obtained from Eq. (37) are

$$E^+ = \langle \psi_+ | H_1 | \psi_+ \rangle = E_d - \frac{3}{16} u^2 N \Delta J,$$

$$E^- = \langle \psi_- | H_1 | \psi_- \rangle = E_d + \frac{3}{16} v^2 N \Delta J. \quad (46)$$

The three processes represented in Figs. 10, 13, and 14 give an extensive negative contribution to  $E^\pm$ . The lack of frustration among these different processes indicates that  $|\psi_+\rangle$  and  $|\psi_-\rangle$  are representative of the VBC orderings, which are stabilized, respectively, for  $\Delta J > 0$  and  $\Delta J < 0$ . We draw particular attention to the fact that in these valence-bond orderings, the four dimers around each uncrossed plaquette resonate between the two configurations shown in Fig. 12. The relative phase is positive on one sublattice ( $A$  for  $\Delta J > 0$  and  $C$  for  $\Delta J < 0$ ) and negative for the other ( $B$  for

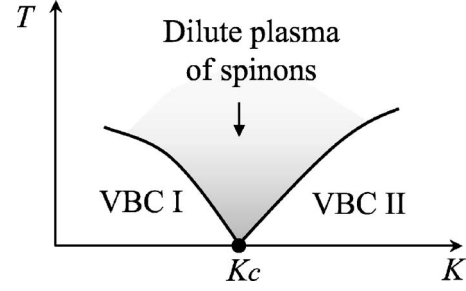


FIG. 16. Low-temperature phase diagram around the Klein point for checkerboard and pyrochlore spin systems.

$\Delta J > 0$  and  $D$  for  $\Delta J < 0$ ). Note that the RK process would lead to a different ground state in which this relative phase is the same for all the plaquettes of the dual lattice. In the pseudospin basis, this corresponds to the ferromagnetic state [ $\vec{q}=(0, 0)$ ] with polarization in the  $\hat{x}$  direction for  $\Delta J < 0$  and the  $-\hat{x}$  direction for  $\Delta J > 0$ .

With regard to possible four-spin perturbation interactions, we remark that the dominant type of such a perturbation would be that contained in the second term of Eq. (1). However, the effect of altering  $K$  is trivially identical to the perturbation of Eq. (23), and the results derived throughout this section may be applied directly to Eq. (1) with a sign inversion of  $\Delta K \equiv (K - K_c)$  relative to  $\Delta J$ .

We now summarize the extension of our results to the pyrochlore lattice. Here, any given dimer covering leads to precisely the same, uniform energy shift (25) when a supplementary nearest-neighbor Heisenberg interaction is inserted. When superpositions of dimer coverings are considered, the elementary graph (or analog of the RK process) circumscribes a hexagon formed by six neighboring tetrahedra. This elementary hexagonal loop replaces the sides of the uncrossed plaquettes on the checkerboard lattice. As for the checkerboard, the graph corresponding to the elementary process is simple, implying that this process is not generated by the perturbation  $H_1$ . Once again, it is necessary to consider larger loops to find the valence-bond ordering stabilized by the perturbation.

As stated above, the local zero-divergence constraint defining the low-energy subspace around the Klein point implies that the low-energy theory induced by a general perturbation is always a compact  $U(1)$  gauge theory. Following the argument of Polyakov, the phase stabilized by a general perturbation is always confining at  $T=0$ . For the spin models we consider, this confining phase consists of a VBC configuration. The perturbation  $H_1$  treated in this section is a particular example of this general observation, and also perhaps the most physically relevant. The effect of a general perturbation in the space of interaction parameters is illustrated in the schematic phase diagram of Fig. 16.

We conclude this section with a summary: we have introduced a loop-based approach to account for the physical processes in short-ranged quantum dimer systems with only local interactions, which is powerful and general. We have used this procedure to compute energies and variational wave functions in the nonorthogonal basis of dimer coverings on the checkerboard lattice. These considerations in-

clude all of the physically relevant perturbations of the Klein Hamiltonian, as discussed in Sec. II, either explicitly or by direct analogy. We conclude that the general case is the one in which VBC phases, which are gapped and confined, are stable away from the Klein point.

## VI. EXACT CRITICALITY IN A FINITE-TEMPERATURE REGION

An issue for the physical properties of a system is rather less the behavior at  $T=0$  than that at finite temperature. In the preceding section, we devised a systematic, purely topological, diagrammatic method to compute the energies of all variational wave functions in the dimer basis. This procedure is exact for the degenerate manifold of (nonorthogonal) basis states and presents a tractable problem at zero temperature as shown in Sec. V. At finite temperatures, the need to evaluate brackets between all possible states in the Hilbert space presents a more serious problem. In this section, we discuss the extent to which progress is possible in this regime by first illustrating how to establish the existence of a finite-temperature region of critical behavior for general perturbations and then consider a simple, anisotropic perturbation to (a) demonstrate explicitly the existence of this critical region and (b) derive its approximate phase boundaries. In the remainder of this section, we set  $k_B=1$  and for rigor assume implicitly that  $J/T \rightarrow \infty$ .  $J$  is the gap scale separating the ground state energies from the lowest excited states. The presence of a spectral gap in a Klein model was shown in Ref. 39.

### A. Finite-temperature criticality

We will consider a general perturbation  $H'$  which augments the Klein-point Hamiltonian to give

$$H_{tot} = H + H'. \quad (47)$$

Equation (23) provides one specific example. We employ the notation  $\epsilon$  (Sec. IV) to denote the small energy scale of  $H'$ . In what follows, we prove that unless the ground states of  $H_{tot}$  are ordered, in the sense that the different ground states are distinguishable by local order parameters, then a region of finite-temperature criticality must occur if the perturbation is not linear in an order parameter.

We begin by stating that the system displays critical correlations (i) when  $\epsilon=0$  at any finite temperature and (ii) at  $T/\epsilon \rightarrow \infty$ . We also note that (iii) any local order parameter vanishes for any fixed  $\epsilon$  at sufficiently high temperatures  $T > T_c(\epsilon)$ . Finally, we assume (iv) that at sufficiently high temperature, the two-point correlator of an order parameter decreases monotonically in temperature at long enough distances. While (i), from Sec. IV, and (iii) are self-evident, the demonstration of statement (ii) represents the core of the proof: because critical correlations appear in the high-temperature limit, (iii) and (iv) imply that correlations at any finite but high enough temperature cannot be weaker than algebraic. Thus, the system exhibits critical correlations at sufficiently high but finite temperature.

The derivation of statement (ii) proceeds from the definition of the relevant order parameter. By analogy with the classical dimer polarization operators presented in Sec. III C, we define the corresponding quantum operators. For a given plaquette  $A$  which is formed by the four sites ( $a$ ,  $b$ ,  $c$ , and  $d$ ) appearing in counterclockwise order, the polarization is given by

$$\begin{aligned} \vec{P}_A &\equiv P_{A;x} \hat{e}_x + P_{A;y} \hat{e}_y + P_{A;z} \hat{e}_z \\ &= [(\vec{S}_a \cdot \vec{S}_d - \vec{S}_b \cdot \vec{S}_c) \hat{e}_x + (\vec{S}_a \cdot \vec{S}_b - \vec{S}_c \cdot \vec{S}_d) \hat{e}_y \\ &\quad + (\vec{S}_a \cdot \vec{S}_c - \vec{S}_b \cdot \vec{S}_d) \hat{e}_z]. \end{aligned} \quad (48)$$

The dimer-dimer correlation function between two crossed plaquettes  $A$  and  $B$  is then given, under the assumption that all states in the Klein manifold are linearly independent<sup>45</sup> and at finite temperatures  $T \gg \epsilon$ , by the expectation value

$$\begin{aligned} \chi_{AB} &= \langle \vec{P}_A \cdot \vec{P}_B \rangle_{\epsilon, T > 0} = \frac{\text{Tr}[e^{-\beta H} \vec{P}_A \cdot \vec{P}_B]}{\text{Tr}[e^{-\beta H}]}, \\ \lim_{T/\epsilon \rightarrow \infty} \chi_{AB} &= \frac{1}{N_g} \sum_{|\psi\rangle} \langle \psi | \vec{P}_A \cdot \vec{P}_B | \psi \rangle \propto |r_{AB}|^{-d}, \end{aligned} \quad (49)$$

with  $|r_{AB}|$  the separation between the centers of the plaquettes  $A$  and  $B$ ,  $d$  the spatial dimensionality,  $N_g$  the number of states in the ground-state manifold (Sec. III A), and the sum taken over a complete set of orthonormal states  $\{|\psi\rangle\}$ . At the Klein point, the correlation function  $\chi_{AB}$  is algebraic, as shown in Sec. IV.

The essential property underlying the physics of the finite-temperature derivation is that the value of  $\chi_{AB}$  is the same for all temperatures when the magnitude  $\epsilon$  of the external perturbation vanishes. This is a consequence of the fact that all states within the Klein-point manifold carry equal weight, wherein  $\chi_{AB}$  is given by the last two lines of Eq. (49) and the system is manifestly critical. As the Klein-point limit is approached for  $T/\epsilon \rightarrow \infty$ , this average becomes equivalent to a sum over all states spanning the Klein-point Hilbert space and its value is precisely the same as for the  $T=0^+$  case when  $\epsilon$  is taken to zero. Here, the probability of any state  $|\psi\rangle$  as given by the finite-temperature density matrix is  $\exp[-\beta E_\psi]/Z = 1/N_g$ . For  $T/\epsilon \rightarrow \infty$ , the correlation function  $\chi_{AB}$  then takes the form specified by Eq. (49), decaying algebraically to 0 as stated in (ii) above.

Although it is not relevant to the above derivation, we remark briefly that topological rules similar to those of Sec. V may be devised for the computation of the dimer-dimer correlation function. As a consequence of the two scalar products appearing in each term of  $\chi_{AB}$ , two permutation operations can be performed on the loop formed by two states (as opposed to the single operation discussed in Sec. V). A similar set of topological rules for the computation of  $\chi_{AB}$  will be provided elsewhere.

The use of statements (ii) and (iii) for arbitrary perturbations is assisted by considering the form of general order parameters. Let  $\{|g_\alpha\rangle\}$  denote the ground states of  $H_{tot}$  and  $\hat{O}$  the order parameter by which they are distinguished. In a

system, which displays local order,  $\hat{O}_{\mathbf{r}}$  is an operator, which depends on a finite number of fields in a sphere (or disk) of finite radius  $R$ , which surrounds a given point  $\mathbf{r}$ . A general algorithm for the construction of the order parameter by examining reduced density matrices is given in Ref. 68.

At  $T=0$  within any ground state,  $\langle \hat{O}_{\mathbf{r}} \hat{O}_{\mathbf{r}'} \rangle \rightarrow |\langle \hat{O}_{\mathbf{r}} \rangle|^2 \equiv m^2 \neq 0$  for separations  $|\mathbf{r}-\mathbf{r}'| \rightarrow \infty$ . Following Eq. (49),

$$\langle \hat{O}_{\mathbf{r}} \rangle = \frac{\sum_{\{\psi, \phi_i\}} \langle \psi | \phi_1 \rangle M_{12} \langle \phi_2 | \hat{O}_{\mathbf{r}} | \phi_3 \rangle M_{34} \langle \phi_4 | \psi \rangle e^{-\beta E_{\psi}}}{\sum_{\psi} e^{-\beta E_{\psi}}}, \quad (50)$$

where  $\{\phi_i\}$  denotes a set of pure dimer states and  $\{\psi\}$  a complete set of orthonormal states spanning the Klein-point basis. Equation (50) makes use of the overcompleteness relation

$$\sum_{\phi_1, \phi_2} |\phi_1\rangle M_{12} \langle \phi_2| = 1_{\text{Klein}}, \quad (51)$$

with  $1_{\text{Klein}} = \prod_{\boxtimes} (1 - \mathcal{P}^{\boxtimes})$  the unit operator in the Klein-point subspace [and  $\mathcal{P}^{\boxtimes}$  the projection operator onto the subspace of net spin  $S_{\boxtimes}=2$  (Sec. II)]. Equation (51) expresses the fact that the dimer states completely exhaust the Klein-point subspace, as proven in Ref. 38. As employed in Ref. 45, all Klein model ground states can be expressed as a sum of projection operators on these ground states, which decompose them into (Young tableaux) sectors, which are well defined under the permutation of pair sites. The presence of a singlet dimer between two sites enforces antisymmetry among the pertinent lattice sites. As evident in expressing the ground states in terms of the irreducible representations of the permutation group, the most general operations allowed within this basis amount to permutations.<sup>69</sup> As the most general permutation can be written as a product of pairwise permutations and as  $\vec{S}_i \cdot \vec{S}_j = \frac{1}{2}(P_{ij} - \frac{1}{2})$ , where  $P_{ij}$  is the operator permuting sites  $i$  and  $j$ , the most general permutation is a functional of scalar spin products. For an operator  $\hat{O}_{\mathbf{r}}$ , which is a functional of spin products of the form  $\vec{S}_a \cdot \vec{S}_b$ , the correlation function  $\langle \hat{O}_{\mathbf{r}} \hat{O}_{\mathbf{r}'} \rangle$  is equivalent to a correlation function between dimer products. From the analogy to a dipolar system (Sec. III), we conclude that the correlation functions containing more scalar spin products decay algebraically according to the strength of the Coulomb interaction between more complicated dipole configurations. Moments of higher order than dipolar are important for those dimers, which are close to each other but far from all other dimers. All correlation functions thus decay algebraically with the dimer-dimer separation. The analysis based on Eq. (49) may now be extended to more general correlation functions, which involve the order-parameter fields  $\hat{O}_{\mathbf{r}}$ .

Returning to statement (iii), as in our earlier considerations for the polarization  $\vec{P}$ , this is based on the result that any finite-temperature expectation value  $\langle \hat{O}_{\mathbf{r}} \hat{O}_{\mathbf{r}'} \rangle$  will decrease monotonically with increasing temperature, and as-

serts that when the expectation value of the order parameter vanishes,  $\langle \hat{O}_{\mathbf{r}} \rangle = 0$ , the corresponding energy scale sets the transition temperature  $T_c$  [(iii)]. This quite universal property is reviewed briefly in Ref. 72. We reiterate [(ii)] the fact that in the high-temperature limit, where correlations are weakest, the correlation function  $\langle \hat{O}_{\mathbf{r}} \hat{O}_{\mathbf{r}'} \rangle$  retains a decay, which is only algebraic in the separation  $|\mathbf{r}-\mathbf{r}'|$ . From these results, it is clear that there is a finite-temperature region surrounding the ‘‘Klein line’’ ( $\epsilon=0, T>0$ ), and explicitly specified by  $T > T_c(\epsilon)$ , where critical correlations appear.

We conclude the general discussion by noting that for a perturbation, which is linear in a general order parameter,  $H' = -\epsilon \sum_A Q_A$ , it is possible that the two-point correlation function takes a finite value,  $\langle Q_A Q_B \rangle \rightarrow m^2 \neq 0$  as  $|r_{AB}| \rightarrow \infty$ , at any finite  $T$ . This type of perturbation may then yield correlations, which are algebraic only in the limit  $T \rightarrow \infty$ .<sup>73</sup> In the next section, we consider a particular perturbation whose effect can be approximated by the anisotropic six-vertex model to show that the dimer correlations may also remain critical up to a threshold value of the perturbation.

## B. Anisotropic perturbation

In this section, we use a specific anisotropic perturbation to investigate the nature of the phase diagram. We will illustrate explicitly that the phase diagram contains a finite-temperature critical region, exemplifying the general concepts of the preceding section, and then derive its approximate phase boundaries.

We consider a perturbation of the form

$$H_d = J_d \sum_{\langle\langle ij \rangle\rangle} \vec{S}_i \cdot \vec{S}_j, \quad (52)$$

where  $\langle\langle ij \rangle\rangle$  denotes all diagonal pairs on the same crossed plaquette. This type of interaction emulates the weakening (for  $J_d < 0$ ) of exchange interactions between neighboring diagonal sites on a checkerboard plaquette relative to those of horizontal or vertical spin pairs, or a lifting (to tetragonal) of the cubic symmetry in a pyrochlore tetrahedron. Focusing for specificity on the checkerboard geometry, for  $H_{\text{tot}} = H + H_d$  it is clear that in the regime  $J_d, T \ll J$ , the effect of  $H_d$  is to favor certain dimer, or equivalently six-vertex, configurations over others, and, in particular, that for  $J_d > 0$  the diagonal contribution  $\langle \psi_a | H_d | \psi_a \rangle$  favors singlet formation on the diagonal bonds of all plaquettes. Because off-diagonal brackets are significantly smaller than diagonal contributions, these may be neglected. The favored ground states in this case are precisely the two antiferroelectric states. Similarly, for  $J_d < 0$ , the single dimer on each crossed plaquette lies preferentially on the vertical or horizontal bonds. Because only the diagonal contributions  $\langle \psi_a | H_d | \psi_a \rangle$  are considered, the ground-state degeneracy for  $J_d > 0$  remains exponentially large: the system supports the subset of all allowed ground states, which corresponds to the ground-state manifold of the Klein model on the square lattice, the size of which scales with  $2^{1+\sqrt{N}}$ , where  $N$  is the number of lattice sites.<sup>7</sup> We remind the reader that the states in this restricted set of dimer coverings, in which precisely one dimer is present on every

square-lattice plaquette, are strictly orthogonal to each other in the thermodynamic limit. The general case has a very much larger manifold of ground states, the classification of which proceeds by the line representation presented in Sec. III.

### 1. Critical region

The illustration that the phase diagram in the presence of this perturbation contains a finite-temperature critical regime is based on the exact limits examined in Sec. VI A and constitutes an explicit implementation of this discussion. We begin by noting, as before, that when  $J_d=0$ , the system remains at the Klein point for all temperatures, displaying critical correlations, and the analysis of Sec. IV is applicable. The susceptibilities  $\chi_{AB}^{aa}=\langle P_{A;a}P_{B;a} \rangle$  are a direct probe of dimer correlations: at  $J_d=0$ , the correlation function  $\chi_{AB}$  is critical for all  $T>0$ .

With reference to the considerations below Eq. (52), for  $J_d>0$ ,  $\chi_{AB}^{zz}$  increases in magnitude relative to its Klein-point value for diagonal dimers only. Thus, (i) the decay of  $\chi$  with distance is no faster than algebraic. However, no VBC order is possible at high temperatures  $T\gg J_d$ , and thus (ii)  $\chi\rightarrow 0$  as the plaquette separation  $|r|\rightarrow\infty$ . Conditions (i) and (ii) taken together imply that for  $T\gg J_d$ , the system exhibits algebraic correlations. Similar considerations apply when  $J_d<0$ , where  $[|\chi_{AB}^{xx}|+|\chi_{AB}^{yy}|]$  increases relative to its Klein-point value, corresponding to correlations of horizontal or vertical dimers. We thus conclude that for  $T\gg |J_d|$ , the system is critical. These statements are completely general, and provide one explanation for why it is that the six-vertex model always has critical, and only critical, correlations at sufficiently high temperatures.<sup>74</sup>

### 2. Finite-temperature criticality by approximate mapping to an anisotropic six-vertex model

We now derive the approximate forms of the phase boundaries of the critical region. This calculation is not exact for the reasons stated at the start of this section, and is included to provide a qualitative indication of the nature of the phase diagram. We begin with an explicit statement of the approximations employed in this derivation. (i) In contrast to Sec. V, for this finite-temperature derivation, the nonorthogonality of the different dimer states is neglected. At the Klein point ( $J_d=0$ ), all dimer configurations carry equal weight and their orthogonality is irrelevant, a fact exploited in Sec. V. All of the properties of the system are a consequence of the entropic considerations presented in Sec. IV. However, away from the Klein point, the configurations no longer have equal probability [in the example of Eq. (52), states with diagonal dimer configurations are favored when  $J_d>0$  and suppressed when  $J_d<0$ ]. (ii) Off-diagonal contributions in the full Hamiltonian, i.e., terms of the form  $\langle \psi_a|H|\psi_b \rangle$  with  $a\neq b$ , are neglected.

When mapped to the six-vertex representation, provided that the conditions  $J_d, T\ll J$  are satisfied, the anisotropic perturbation of Eq. (52) is reflected in a change in the relative weights of the six-vertex configurations (which at low temperatures are the only states with nonvanishing weights). At

$T=0$ , for  $J_d>0$ , these nonuniform weights are represented by vanishing energies for four of the vertex types while the other two contribute an equal and finite energy, and conversely for  $J_d<0$ .

With reference to Fig. 3, we choose the energies of the six-vertex configurations displayed to be  $\epsilon_{i=1,2,3,4}=0$  and  $\epsilon_5=\epsilon_6=-\frac{3}{4}J_d$  in the presence of the perturbation. The correlations and thermodynamics of this model are best analyzed through the fugacities  $a=\exp[-\beta\epsilon_1]=\exp[-\beta\epsilon_2]$ ,  $b=\exp[-\beta\epsilon_3]=\exp[-\beta\epsilon_4]$ , and  $c=\exp[-\beta\epsilon_5]=\exp[-\beta\epsilon_6]$ , where  $\beta$  is the inverse temperature. The fugacities determine a parameter  $\Delta$  whose value determines, in turn, the phase in which the six-vertex model lies,

$$\Delta = \frac{a^2 + b^2 - c^2}{2ab}. \quad (53)$$

Following Lieb's original solution of the six-vertex model,<sup>42,43</sup> all models with  $|\Delta|<1$  are in the disordered phase. Such small- $|\Delta|$  systems, including the ice model relevant for the isotropic checkerboard lattice where  $a=b=c=1$ , are in the disordered phase and exhibit power-law correlations. By contrast, for  $\Delta>1$ , the system adopts an ordered configuration where all arrows have a definite chirality (such as up and to the right or down and left). In the system with perturbation  $J_d$ ,  $a=b=1$  while  $c=\exp[\frac{3}{4}\beta J_d]$ , and one finds that if

$$T > \frac{3}{8 \ln 2} J_d, \quad (54)$$

then  $|\Delta|<1$ , indicating that the system is in its disordered phase. In this case, we find power-law correlations among dimer pairs and the system is trivially critical for all nonzero temperatures when  $J_d<0$ , or critical only at sufficiently high temperatures [whose lower bound is given by Eq. (54)] whenever  $J_d>0$ . When  $T=0$ , one finds that for all  $J_d<0$ , the system lies precisely on the boundary between the ordered and the critical phase ( $\Delta=1$ ). Equation (54) defines a finite region within the  $(J_d, T)$  plane (Fig. 17) in which the system is critical.

The above results are applicable under the conditions that all relevant states lie within the Klein basis manifold, i.e.,  $T\ll J$ , that the effects of nonorthogonality are neglected, and that only the diagonal corrections induced by  $H_d$  are considered. Although these are small, off-diagonal contributions of the type  $\langle \psi_a|H_d|\psi_b \rangle$  analogous to those computed in Sec. V are relevant in removing the "marginally critical"  $T=0$  correlations obtained for  $J_d<0$ , and stabilize once again a particular valence-bond ordering pattern of the types considered in detail in Sec. V. In this situation, the marginally critical line may be moved to finite temperatures, separating the low- $T$  ordered phase from a finite- $T$  critical regime. In summary, it is possible to demonstrate rigorously that specific types of perturbation around the Klein point lead to an exotic, exactly critical regime. Quantitative calculations of the properties of this regime are not exact, but approximations of the kind applied here may be used for the qualitative determination of quantities such as the boundaries of this phase.

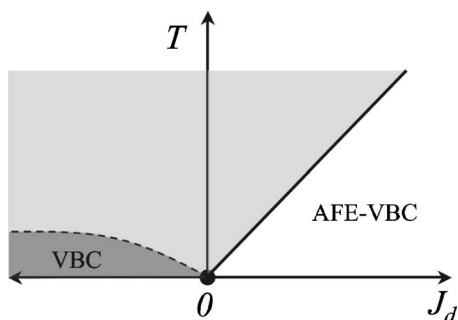


FIG. 17. Approximate phase diagram for the Klein-point Hamiltonian with diagonal exchange perturbation  $J_d$ . Neglecting both nonorthogonality and off-diagonal contributions, an antiferroelectric valence bond crystal (AFE-VBC) ordering is stabilized below  $T=3J_d/(8 \ln 2)$  for  $J_d>0$ . The system is critical at all points within the region shaded in light gray. In the absence of off-diagonal processes, it remains critical to zero temperature for  $J_d<0$ ; the qualitative effect of these processes is to remove the low-temperature critical behavior by stabilizing a VBC ordering in the region shaded dark gray. While the phase boundaries shown above are approximate, the existence of a finite-temperature critical region is not (Sec. VI A).

## VII. DISCUSSION AND CONCLUSIONS

The pyrochlore ( $A_2B_2O_7$ ) and spinel ( $AB_2O_4$ ) structures are very common among magnetic oxides, occurring for a wide variety of transition and rare-earth metals such as both the  $A$  and  $B$  ions and thereby offering a range of valence states and magnetic moments  $S$  in a pyrochlore lattice of interacting spins. Because the orbital contribution to the magnetic moment of transition-metal ions in the  $3d$  series is quenched by the crystal-field splitting, the spin-orbit coupling has only a perturbative effect and the relevant physical spin models are effectively  $SU(2)$  invariant. While the link to a physical pyrochlore or spinel system satisfying all the necessary criteria remains to be found (Sec. II), we have shown here that for these structures, a class of  $SU(2)$ -invariant  $S=1/2$  models of this type, whose local interactions emerge directly from the simplest Hubbard Hamiltonian, gives rise to spinon excitations, which propagate in the full lattice.

At the root of the exotic behavior exhibited by this type of system is the massive (extensive) degeneracy of the ground-state manifold in the vicinity of the Klein critical point. We have gained physical insight into the multiple essential aspects of this problem by exploiting exact mappings between the spin system under consideration and other physical systems.<sup>75</sup> In particular, because the ground-state sector of the  $S=1/2$  Klein models on the pyrochlore lattice obeys ice rules of the type discussed in Sec. III, it is possible to exploit analogies with six-vertex models,<sup>42</sup> string gases, and  $U(1)$  gauge magnets to make a number of powerful qualitative and quantitative statements. The local constraint of zero divergence imposed by the ice rules implies that the low-energy sector is described by an effective  $U(1)$  gauge theory in the neighborhood of the Klein point. This theory is, however, not necessarily the minimal  $U(1)$  gauge magnet, whose terms involve only the smallest loops, which is usually invoked in these cases.<sup>20</sup> The variational approach, which we introduce

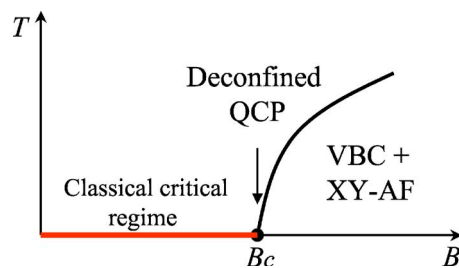


FIG. 18. (Color online) Low-temperature phase diagram for the Klein Hamiltonian in the presence of a Zeeman term (applied magnetic field  $B$ ) for the checkerboard and pyrochlore spin systems.

and employ in Sec. V indicates that in some cases, as a result of the nonorthogonality of the singlet dimer coverings, processes involving larger loops are relevant for realistic physical perturbations.

Although the spinons are deconfined excitations only at a single point (the Klein point) of the quantum phase diagram ( $T=0$ ), this deconfinement exists over a finite region of the phase diagram due to thermal fluctuations, which give rise to a dilute plasma phase of spinons. The spinon-spinon correlations in this region are dominated by the  $T \rightarrow 0^+$  Klein critical point, whose critical fluctuations are of entropic origin. The primary characteristic of the Klein point is the stabilization of a low-energy manifold of states satisfying a local constraint of zero divergence, or equivalently the ice rules,<sup>10,11</sup> and the removal of any low energy scale. As a consequence of both conditions, the system becomes critical due to entropic fluctuations induced even at infinitesimal temperatures.

These features are directly relevant for the potential observation of spinons in two- or three-dimensional systems. In the case of the pyrochlore lattice models considered here, the deconfined phase is expected to appear near a transition between two valence-bond crystals. Similar considerations were applied to the  $S=1/2$  model studied in Ref. 7, the difference in that case being that the spinons propagate along one-dimensional paths because the dimensional reduction at the corresponding Klein point is incomplete.

It is also interesting to note that an exact deconfined quantum critical point<sup>5</sup> (QCP) can be induced by adding a Zeeman term to the Klein Hamiltonian of Eq. (8). The QCP is induced at the critical magnetic field  $B_c$ , which closes the singlet-triplet spin gap. The excited two-spinon deconfined state becomes the ground state at  $B_c$ . For higher values of the field ( $B>B_c$ ), the concentration of spinons becomes finite and the degeneracy between the underlying singlet dimer coverings is lifted. Consequently, spinon-spinon confinement is restored and the resulting triplet pairs are expected to condense, giving rise to an  $XY$ -type antiferromagnet ( $XY$ -AF) in the plane perpendicular to the applied field.

In the presence of a magnetic field, the system at the Klein point displays a true deconfined QCP between a line of classical critical points in the region  $B<B_c$  and a magnetically ordered region at  $B>B_c$  with two coexisting order parameters. A schematic phase diagram illustrating the finite extent of the deconfined regime is shown in Fig. 18. Very different and much more conventional behavior is obtained

away from the Klein point, where the ground-state degeneracy is lifted. Here, the region  $B < B_c$  has a VBC ground state with gapped magnon excitations separated by a conventional QCP from an ordered phase with spin-wave excitations.

The ideas and concepts connected with deconfinement at quantum critical points have formed an extensive recent literature best summarized in Ref. 5. As noted in Sec. I, many of these studies depart from effective  $U(1)$  gauge-theoretical treatments rather than microscopic models, and it is not yet clear that specific systems exist, which realize the desired deconfinement properties. The Klein point in certain pyrochlore lattice models was considered briefly in Ref. 39, although these authors did not dwell on either the detailed physical properties of such a point or on their origin. We have found that the mapping used in this study to a quantum dimer model with only RK interactions is not, in fact, justified for a Heisenberg antiferromagnet in a pyrochlore geometry. The scenario of the “constrained entropic critical point” introduced recently in Ref. 76 contains certain parallels to the physics of the Klein point with regard to high-temperature constraints. However, this is said to be a “top-down” construction based on different energy scales, some of which are present in a number of the effective models considered, and does not contain specific properties emerging from a microscopic Hamiltonian for all temperature regimes.

We conclude this discussion with a speculation. The exponential ground-state degeneracy [Eqs. (12) and (14)] and the resulting extensive configurational entropy, which we have found suggest, but certainly do not mandate, that glassy spin dynamics may occur naturally in pyrochlores. We stress that these systems are uniform and disorder-free but frustrated, wherein this suggestion would reinforce the widely held belief that frustration rather than disorder is the fundamental requirement for the dynamical properties of structural glasses. The basic premise of the Vogel-Fulcher (VF) form of glassy dynamics is that the relaxation times appear to diverge at a temperature which correlates well with the intercept ( $T_0$ ) of the extrapolated entropy of the supercooled liquid to that of the solid. According to a prevalent line of reasoning,<sup>77</sup> as the system is cooled, the configurational entropy first becomes extensive at  $T_A$ , the onset temperature of multiple local free-energy minima; at a lower temperature,  $T_0$ , these minima become stable and the configurational entropy vanishes. If an exponentially large number of metastable states are found for  $T_A > T > T_0$ , one may invoke the analysis of entropic droplets<sup>77</sup> to obtain the characteristic free-energy barrier height

$$\Delta E \propto (TS_c)^{-1}. \quad (55)$$

Linearizing the extensive configurational entropy,

$$S_c(T \rightarrow T_0^+) \sim V(T/T_0 - 1), \quad (56)$$

leads to VF dynamics<sup>77</sup> with relaxation times

$$\tau \sim \exp[DT_0/(T - T_0)]. \quad (57)$$

Here,  $T_0$  is a temperature scale close to the Kauzmann temperature<sup>78</sup> at which an “ideal glass transition” would occur, and where the extrapolated entropy of the assumed liq-

uid undergoes a crisis. We stress that this very general derivation of a systematic definition for glassy behavior, by consideration of free-energy barriers,<sup>77</sup> does not require that the different ground states be linked only by infinite-length processes. (However, if only the spatially longest processes were operational, this would indeed lead to very robust, exponentially slow quantum dynamics, as first noted by Chamon and co-workers.<sup>79</sup>) For the pyrochlore system we have shown that there exist finite-length tunneling processes linking different ground states within the highly degenerate low-energy sector, thus suggesting an obvious candidate system for this type of glass. We comment that the physical processes indicated here, namely, of glassy spin dynamics arising from frustration in a periodic lattice, are similar to early ideas of the “topological spin glass” of Ref. 80. Empirically, glassy dynamics is strongly indicated in a number of frustrated magnetic systems, of which we quote only a selective list: evidence of phases with certain glassy characteristics has been reported in some pyrochlores, including  $Y_2Mo_2O_7$ ,<sup>81,82</sup> in the stacked kagome layer system  $SrCr_{8,6}Ga_{3,4}O_{19}$  (Ref. 82) and in the kagome bilayer compound  $Ba_2Sn_2ZnCr_{6,8}Ga_{3,2}O_{22}$ .<sup>83</sup> Further indications for glassy behavior are found in some quasitriangular antiferromagnets, including  $NiGa_2S_4$ .<sup>84</sup>

In conclusion, we have performed a detailed analysis of a physically motivated quantum spin model with only near-neighbor interactions on the two- and three-dimensional pyrochlore lattices. This reveals a wealth of exotic behavior, which can be traced to the extensive degeneracy of the system at the Klein point and thus to a complete dimensional reduction. The complete absence of quantum fluctuations in the ground-state manifold at the Klein point leads to another type of classical critical point, with exactly known critical behavior, which we stress emerges from a highly frustrated, microscopic quantum spin model.

The critical correlations at the Klein point are driven by entropic (thermal) fluctuations, leading to an effective plasma phase with Coulombic interactions. These are not confining, when the elementary excitations are deconfined spinons which propagate freely in all directions (a further manifestation of complete dimensional reduction). This high-dimensional fractionalization would also be manifested as a spin-charge separation in the dilute limit of added holes if the carrier hopping were much smaller than the magnetic energy scale  $J$ . Physically relevant perturbations away from the Klein point lead, in general, to confined phases of static valence-bond order with spin gaps to  $S=1$  excitations. However, at finite temperatures in the vicinity of the Klein point, the classical criticality is dominant and deconfinement persists over a finite region of the phase diagram. This type of deconfined behavior goes well beyond the simple, thermal decoupling of a system (to obtain quasi-one-dimensional behavior) in that the classical critical point is driven to  $T=0^+$ : the microscopic origin of deconfinement lies in the proximity of the system to a Klein point, and spinon propagation remains  $d$  dimensional.

We have obtained our conclusions and, as a result, a rather complete picture of a distinctive paradigm for classical and quantum criticalities, from a number of rigorous techniques. The dimer coverings of the checkerboard and pyro-

chlore lattices may be treated, through their connection with the ice rules, by both the six-vertex mapping and a line representation, which exploit the underlying topological order of the physical system to classify the states of the manifold. We have developed a loop representation of the physical processes in the dimer basis, which has very general applicability to calculations involving the nonorthogonal dimer states; this gives a clear and intuitive picture of all contributing local processes, as reflected in the sizes of corresponding loops, and a straightforward but rigorous set of rules systematizing their computation.

Recently, Pollmann *et al.* reported, in a series of preprints,<sup>85</sup> on a spinless Fermi model, which possesses sev-

eral of the qualitative features, which we found here for spin systems on the pyrochlore and checkerboard lattices.

### ACKNOWLEDGMENTS

We thank B. Kumar for helpful discussions. We also wish to thank F. Pollmann and K. Shtengel for their enthusiastic interest and for encouraging us to emphasize the absence of the Rokhsar-Kivelson type processes in our bare systems. This work was sponsored by the U.S. DOE under Contract No. W-7405-ENG-36 and by PICT 03-06343 of the ANP-CyT of Argentina.

- 
- <sup>1</sup>P. W. Anderson, G. Baskaran, Z. Zou, and T. Hsu, *Phys. Rev. Lett.* **58**, 2790 (1987).
- <sup>2</sup>A. M. Polyakov, *Nucl. Phys. B* **120**, 429 (1977).
- <sup>3</sup>S. Sachdev and K. Park, *Ann. Phys. (N.Y.)* **298**, 58 (2002); I. F. Herbut, B. H. Seradjeh, S. Sachdev, and G. Murthy, *Phys. Rev. B* **68**, 195110 (2003).
- <sup>4</sup>M. Hermele, T. Senthil, M. P. A. Fisher, P. A. Lee, N. Nagaosa, and X-G. Wen, *Phys. Rev. B* **70**, 214437 (2004).
- <sup>5</sup>T. Senthil, A. Vishwanath, L. Balents, S. Sachdev, and M. P. A. Fisher, *Science* **303**, 1490 (2004), and references therein.
- <sup>6</sup>C. D. Batista and Z. Nussinov, *Phys. Rev. B* **72**, 045137 (2005).
- <sup>7</sup>C. D. Batista and S. A. Trugman, *Phys. Rev. Lett.* **93**, 217202 (2004).
- <sup>8</sup>A. P. Ramirez, *Annu. Rev. Mater. Sci.* **24**, 453 (1994).
- <sup>9</sup>H. Takagi, [http://online.itp.ucsb.edu/online\\_exotic\\_04/takagi/pdf/Takagi.pdf](http://online.itp.ucsb.edu/online_exotic_04/takagi/pdf/Takagi.pdf).
- <sup>10</sup>D. Bernal and R. H. Fowler, *J. Chem. Phys.* **1**, 515 (1933).
- <sup>11</sup>L. Pauling, *The Nature of the Chemical Bond* (Cornell University Press, Ithaca, 1939).
- <sup>12</sup>R. Moessner, *Can. J. Phys.* **79**, 1283 (2001), and references therein; R. Moessner and J. T. Chalker, *Phys. Rev. Lett.* **80**, 2929 (1998).
- <sup>13</sup>B. Canals and C. Lacroix, *Phys. Rev. Lett.* **80**, 2933 (1998).
- <sup>14</sup>S. T. Bramwell and M. J. P. Gingras, *Science* **294**, 1495 (2001), and references therein.
- <sup>15</sup>We provide a brief summary of the selected contributions to the pyrochlore problem. The case of an Ising antiferromagnet on a pyrochlore lattice was investigated by Anderson (Ref. 16), who noted the similarity to the spin-ice problem. Analytical treatments of this model (Ref. 17) have yielded the precise form of the correlation functions, which have been confirmed by numerical studies (Ref. 18). The classical antiferromagnet has been investigated by the large- $N$  technique (Ref. 19), and quantum Heisenberg spins on the pyrochlore structure have been addressed in a number of studies (Refs. 20 and 21) by perturbative treatments based on the Ising result with sufficiently large transverse terms. These approaches lead to the rich physics of ring-exchange interactions (Refs. 20 and 21), as well as to a rather elegant charge model (Ref. 22), and suggest the strong possibility of fractionalized excitations. While some approaches (Ref. 13) indicate the absence of spin order in the quantum pyrochlore antiferromagnet, numerical studies suggest specific singlet ordering patterns for the ground states of certain  $S=1/2$  antiferromagnetic models (Refs. 25–27). Specific results for simple, microscopic, isotropic, nearest-neighbor quantum spin Hamiltonians are lacking. Contradicting the support for fractionalization, the large- $S$  technique suggests for the classical Heisenberg antiferromagnet on the pyrochlore and checkerboard lattices (Refs. 23 and 24) that magnetic order may be established at low temperatures, driven by an order-by-disorder (Refs. 12 and 28) effect where tunneling between states lifts the classical ground-state degeneracy and stabilizes order. Recent studies (Ref. 29) of systems similar to the effective spin models of Ref. 27 have provided rigorous demonstrations of this effect for the classical case (i.e., with thermal rather than quantum fluctuations).
- <sup>16</sup>P. W. Anderson, *Phys. Rev.* **102**, 1008 (1956).
- <sup>17</sup>J. Villain, *Solid State Commun.* **10**, 967 (1972); F. H. Stillinger and M. A. Cotter, *J. Chem. Phys.* **58**, 2532 (1973); R. W. Youngblood and J. D. Axe, *Phys. Rev. B* **23**, 232 (1981); L. B. Ioffe and A. I. Larkin, *ibid.* **40**, 6941 (1989); D. A. Huse, W. Krauth, R. Moessner, and S. L. Sondhi, *Phys. Rev. Lett.* **91**, 167004 (2003); C. L. Henley, *Phys. Rev. B* **71**, 014424 (2005).
- <sup>18</sup>S. Yoshida, K. Nemoto, and K. Wada, *J. Phys. Soc. Jpn.* **71**, 948 (2002).
- <sup>19</sup>D. A. Garanin and B. Canals, *Phys. Rev. B* **59**, 443 (1999); B. Canals and D. A. Garanin, *Can. J. Phys.* **79**, 1323 (2001).
- <sup>20</sup>M. Hermele, M. P. A. Fisher, and L. Balents, *Phys. Rev. B* **69**, 064404 (2004).
- <sup>21</sup>N. Shannon, G. Misguich, and K. Penc, *Phys. Rev. B* **69**, 220403(R) (2004).
- <sup>22</sup>P. Fulde, K. Penc, and N. Shannon, *Ann. Phys.* **11**, 892 (2002).
- <sup>23</sup>O. Tchernyshyov, O. A. Starykh, R. Moessner, and A. G. Abanov, *Phys. Rev. B* **68**, 144422 (2003).
- <sup>24</sup>U. Hizi, P. Sharma, and C. L. Henley, *Phys. Rev. Lett.* **95**, 167203 (2005).
- <sup>25</sup>R. Moessner, O. Tchernyshyov, and S. L. Sondhi, *J. Stat. Phys.* **116**, 755 (2004).
- <sup>26</sup>B. Canals, *Phys. Rev. B* **65**, 184408 (2002).
- <sup>27</sup>E. Berg, E. Altman, and A. Auerbach, *Phys. Rev. Lett.* **90**, 147204 (2003).
- <sup>28</sup>J. Villain, R. Bidaux, J. P. Carton, and R. Conte, *J. Phys. (Paris)* **41**, 1263 (1980); E. F. Shender, *Sov. Phys. JETP* **56**, 178 (1982).
- <sup>29</sup>Z. Nussinov, M. Biskup, L. Chayes, and J. van den Brink, Euro-

phys. Lett. **67**, 990 (2004); M. Biskup, L. Chayes, and Z. Nussinov, *Commun. Math. Phys.* **255**, 253 (2005).

<sup>30</sup> Antiferromagnetic nearest-neighbor interactions on the pyrochlore lattice have a strong, intrinsic geometrical frustration. For both classical and quantum spins, it is impossible to bring all the individual exchange interactions close to their minimal value simultaneously. The competition of individual Heisenberg interactions is exacerbated by the inclusion of the symmetric four-spin interaction. The extent of the frustration can be characterized quite generally by the ground-state degeneracy, and this is maximized at the point  $K=K_c=4J/5$ . A discussion of the nature of the level crossing occurring at this point is contained in Sec. V.

<sup>31</sup> The reader may wish to verify the mapping between Eqs. (1) and (2) by application of the standard  $S=1/2$  identities as follows:

$$\{(\vec{S}_i \cdot \vec{S}_j), (\vec{S}_i \cdot \vec{S}_k)\} = \frac{1}{2}(\vec{S}_i \cdot \vec{S}_k), \quad j \neq k,$$

$$(\vec{S}_i \cdot \vec{S}_j)^2 = \frac{3}{16} - \frac{1}{2}(\vec{S}_i \cdot \vec{S}_j). \quad (58)$$

The first relation follows from the anticommutation of different spin components at a single lattice site,

$$\{S_i^a, S_i^b\} = \frac{1}{2}\delta_{ab}, \quad a, b = x, y, z, \quad (59)$$

and the second follows, among other derivations, from the identity  $\vec{S}_i \cdot \vec{S}_j = \frac{1}{2}(P_{ij} - \frac{1}{2})$ , where  $P_{ij}$  is the operator permuting sites  $i$  and  $j$ .

<sup>32</sup> In the case of the checkerboard lattice, there is also a biquadratic spin term, which involves the four sites of each uncrossed plaquette. These processes are not included in the Hamiltonian of Eq. (2).

<sup>33</sup> E. Müller-Hartmann and A. Reischl, *Eur. Phys. J. B* **28**, 173 (2002).

<sup>34</sup> A. A. Katanin and A. P. Kampf, *Phys. Rev. B* **66**, 100403(R) (2002); A. A. Katanin and A. P. Kampf, *Phys. Rev. B* **67**, 100404(R) (2003).

<sup>35</sup> A. Chubukov, E. Gagliano, and C. Balseiro, *Phys. Rev. B* **45**, 7889 (1992).

<sup>36</sup> This lies outside the range of validity of  $\tilde{H}_{\text{Hubb}}$  as an effective low-energy Hamiltonian for  $H_{\text{Hubb}}$  [ $J_1 = -J_2$  for  $t/U = 1/\sqrt{30}$  to  $\mathcal{O}(t^4/U^3)$ ]. However, the Klein condition  $J_1 = -J_2$  can be obtained for smaller values of  $t/U$ , such that  $\tilde{H}_{\text{Hubb}}$  becomes a valid description of the low energy spectrum, if a ferromagnetic nearest-neighbor direct exchange interaction is added to the Hubbard model. Such a direct exchange contribution is always present in real systems.

<sup>37</sup> D. J. Klein, *J. Phys. A* **15**, 661 (1982). For completeness, we remark that Klein's original work examined the total spin formed by sites which surround a given lattice site. This is slightly different than the case we examine in our work. Here, the projection operators act on the total spin of all sites, compromising a basic building block such as the tetrahedron. Such a similar extended idea was employed in Ref. 7.

<sup>38</sup> Z. Nussinov, cond-mat/0606075 (unpublished).

<sup>39</sup> K. S. Raman, R. Moessner, and S. L. Sondhi, *Phys. Rev. B* **72**, 064413 (2005).

<sup>40</sup> L. Onsager and M. Dupuis, in *Thermodynamics of Irreversible Processes*, Proceedings of the International of Physics "Enrico Fermi," Course X, Varena, 1959, edited by S. R. De Groot (Societa Italiana di Fisica, Bologna, 1960); B. Simon, *The Statistical Mechanics of Lattice Gases* (Princeton University Press, Princeton, NJ, 1993), Vol. I, p. 315.

<sup>41</sup> J. F. Nagle, *J. Math. Phys.* **7**, 1484 (1966).

<sup>42</sup> R. J. Baxter, *Exactly Solved Models in Statistical Mechanics* (Academic, London, 1982).

<sup>43</sup> E. H. Lieb, *Phys. Rev.* **162**, 162 (1967).

<sup>44</sup> Two arbitrary states are in general nonorthogonal, but their overlap is exponentially small in the length of closed loops obtained by superposing them. Linear independence of singlet dimer coverings has been proven for other lattices in Ref. 45.

<sup>45</sup> J. T. Chayes, L. Chayes, and S. A. Kivelson, *Commun. Math. Phys.* **123**, 53 (1989). It should be noted that the conclusions presented in our work remain unchanged even if not all dimer states were linearly independent [a fact which was proved in the work of J. T. Chayes *et al.* for several (but not all) lattices]. Our analysis will hold so long as the number of linearly independent states scales linearly with the number of dimer coverings which are ground states of Klein type Hamiltonians.

<sup>46</sup> A schematic of such states on the square lattice can be found in Figs. 1(c) and 1(d) of Ref. 7; these are also allowed states of the ground-state manifold on the checkerboard lattice.

<sup>47</sup> We assume here that the diagonal elements of the perturbative term  $H'$  do not break the degeneracy; this would be the case when, for example,  $H'$  is a Heisenberg Hamiltonian of the type given by the first term of  $H$ .

<sup>48</sup> X.-G. Wen, *Quantum Field Theory of Many-Body Systems* (Oxford University Press, Oxford, 2004).

<sup>49</sup> I. Affleck, T. Kennedy, E. H. Lieb, and H. Tasaki, *Commun. Math. Phys.* **115**, 477 (1988).

<sup>50</sup> T. Kennedy and H. Tasaki, *Commun. Math. Phys.* **147**, 431 (1992).

<sup>51</sup> P. W. Kasteleyn, *Physica (Amsterdam)* **27**, 1209 (1961); P. W. Kasteleyn, *J. Math. Phys.* **4**, 287 (1963).

<sup>52</sup> M. E. Fisher, *Phys. Rev.* **124**, 1664 (1961); P. W. Kasteleyn, *Physica (Amsterdam)* **27**, 1209 (1961); M. E. Fisher and J. Stephenson, *Phys. Rev.* **132**, 1411 (1963).

<sup>53</sup> In contrast to the mappings between quantum spin and dimer models, the orthogonality between different dimer coverings is not a requirement in this case because the effective spinon-spinon interaction has an entropic origin and the entropy is determined solely by the number of linearly independent states.

<sup>54</sup> J. B. Kogut, *Rev. Mod. Phys.* **51**, 659 (1979); E. Fradkin and S. H. Shenker, *Phys. Rev. D* **19**, 3682 (1979).

<sup>55</sup> A. H. Castro Neto, P. Pujol, and E. Fradkin, *Phys. Rev. B* **74**, 024302 (2006).

<sup>56</sup> W. Krauth and R. Moessner, *Phys. Rev. B* **67**, 064503 (2003).

<sup>57</sup> The energies of Eq. (2) when evaluated for a single tetrahedron at  $K=K_c + \delta K$  are

$$E_{S_{\text{tet}}=0} = 0,$$

$$E_{S_{\text{tet}}=1} = \frac{5}{4}\delta K,$$

$$E_{S_{\square}=2} = \frac{12}{5}J - \frac{3}{4}\delta K, \quad (60)$$

for the singlet, triplet, and quintet states, respectively. For  $|\delta K| \ll J$ , the energy difference between the singlet and triplet states is much smaller than the gap to the quintet state.

<sup>58</sup>R. E. Peierls, *Phys. Rev.* **54**, 918 (1938).  
<sup>59</sup>H. Kleinert, *Gauge Fields in Condensed Matter Physics* (World Scientific, Singapore, 1989).  
<sup>60</sup>J. Villain, *J. Phys. (Paris)* **36**, 581 (1975).  
<sup>61</sup>J. Zaanen, Z. Nussinov, and S. Mukhin, *Ann. Phys.* **310**, 181 (2004); V. Cvetkovic, Z. Nussinov, and J. Zaanen, *cond-mat/0508664*, *Philos. Mag. B* (to be published).  
<sup>62</sup>E. Fradkin, *Field Theories of Condensed Matter Systems* (Addison-Wesley, Boston, 1994), and references therein.  
<sup>63</sup>G. Rumer, *Nachr. Ges. Wiss. Goettingen, Math.-Phys. Kl.* **1932**, 337; S. Liang, B. Doucot, and P. W. Anderson, *Phys. Rev. Lett.* **61**, 365 (1988); B. Sutherland, *Phys. Rev. B* **37**, 3786 (1988); M. Kohmoto and Y. Shapir, *ibid.* **37**, 9439 (1988); R. McWeeny, in *Valence Bond Theory and Chemical Structure*, Studies in Physical and Theoretical Chemistry, Vol. 64, edited by D. J. Klein and N. Trinajstic (Elsevier, Amsterdam, 1990), p. 13; M. Havelio, *Phys. Rev. B* **54**, 11929 (1996).  
<sup>64</sup>S. A. Kivelson, D. S. Rokhsar, and J. P. Sethna, *Phys. Rev. B* **35**, 8865 (1987); D. S. Rokhsar and S. A. Kivelson, *Phys. Rev. Lett.* **61**, 2376 (1988).  
<sup>65</sup>A separate algorithm for the computation of energies and correlation functions in valence-bond states was developed shortly after this work, by K. S. D. Beach and A. W. Sandvik, *Nucl. Phys. B* **750**, 142 (2006). The approach of these authors does not apply the topological rules exploited here, but offers insight into a number of other related points.  
<sup>66</sup>D. Horn, *Phys. Lett.* **100B**, 149 (1981).  
<sup>67</sup>R. Moessner and S. L. Sondhi, *Phys. Rev. B* **63**, 224401 (2001).  
<sup>68</sup>S. Furukawa, G. Misguich, and M. Oshikawa, *Phys. Rev. Lett.* **96**, 047211 (2006).  
<sup>69</sup>An introductory exposition to the Young tableaux is available in many texts (e.g., Refs. 70 and 71). Each of the Klein model ground states is a superposition of a product of singlets (Ref. 38). In the Young tableaux notation, these ground states therefore lie exclusively in the two row sector in which the length of both rows is the same. The top row labels in the Young tableaux denote sites in which up spins are antisymmetrized (to form singlet dimers) with down state spins belonging to site indices in the row just below it. Now, consider any of these ground states ( $\{|\psi_j\rangle\}$ ). In order for an operator  $V$  acting on these states ( $V|\psi_j\rangle$ ) to lie in the same Young tableaux sector and allow for finite matrix elements  $\langle\psi_i|V|\psi_j\rangle$  in the Klein ground-state basis, we must have that  $V$  merely permutes the site indices on the top and bottom rows. The operator  $V$  can, of course, also do nothing at all (and act as the identity); this is the case for a uniform rotation operator, which leaves the Klein spin state invariant. [After all, any Klein basis spin state is a global singlet ( $S_{tot}=0$ ) as it is a superposition of a product of singlet dimers.] Thus, the most general operator  $V$ , which has nonvanishing matrix elements in the Klein ground-state basis has components, which are the superposition of the most general permutation operations (including the trivial permutation—the identity operator). We re-emphasize that this follows as (i) the different Young tableaux

sectors are orthogonal to one another and that (ii) within the Young tableaux pertinent to the Klein basis sector, all sites on the top row of the tableaux lie in the up-spin state while all sites in the bottom row (whose length is equal to that of the top row) are indexed by a down-spin state. No operators  $V$  other than those involving a sum of permutations can link states in this Young tableaux sector.

<sup>70</sup>J. J. Sakurai, *Modern Quantum Mechanics* (Addison-Wesley, Reading, MA, 1985), Chap. 6.  
<sup>71</sup>Wu-Ki Tung, *Group Theory in Physics* (World Scientific, Singapore, 1985), Chaps. 5 and 13.  
<sup>72</sup>In the absence of external symmetry-breaking fields, the competition of energy and entropy is resolved universally in favor of disorder at sufficiently high temperatures (symmetry restoration). We summarize those parts of the physical origin of this phenomenon most relevant to the current considerations. General disordering events (similar to those in Sec. IV) have positive energy penalties ( $\Delta E$ ) and entropy gains ( $\Delta S$ ). At sufficiently high temperatures  $T$ , the free-energy change due to the increase in disordering processes,  $\Delta F = \Delta E - T\Delta S$ , becomes negative: defects proliferate and order is destroyed. For general, discrete order parameters in a system of finite-range interactions, the scaling of  $\Delta E$  with defect (domain-wall) size is no faster than that of  $\Delta S$ , where domain-wall deconfinement leads to a lower free energy at sufficiently high  $T$ . For continuous order parameters there exist further lower-energy deformations in addition to domain walls, which are already favorable. Thus, there is always a temperature  $T_c$  beyond which the free energy is lowered monotonically by contributions from disorder-increasing processes. As a consequence, for  $T > T_c$ , the expectation value  $\langle\hat{O}_r\rangle = 0$ .  
<sup>73</sup>The development of long-range order in  $Q$  [ $m \equiv \langle Q_A \rangle \neq 0$  at all finite  $T$ ] in this case is not in conflict with finite-temperature singularities in the free energy, which may lead to algebraic correlations in quantities other than  $Q$ . One example is afforded by the classical six-vertex model in any symmetry-breaking field, which is analogous to the parameter  $\epsilon$  in  $H'$ . In this model the field may cause all six states to have different energies, but criticality appears nevertheless at finite fields and temperatures [see, for example, Fig. 8.6 in Ref. 42].  
<sup>74</sup>We should remark that this finite  $T$  critical behavior is distinct from the exact deconfinement present at  $T=0$  albeit very similar to it. At  $T > 0$ , the entropic contribution ( $-T\Delta S$ ) to the free energy leads to an effective (marginally confining) logarithmic interaction between monomers at the ice point. However, as discussed in Sec. IV, this logarithmic interaction is screened (by virtue of a finite defect concentration at  $T > 0$ ) at sufficiently large distances.  
<sup>75</sup>C. D. Batista and G. Ortiz, *Adv. Phys.* **53**, 1 (2004).  
<sup>76</sup>C. Castelnovo, C. Chamon, C. Mudry, and P. Pujol, *Phys. Rev. B* **73**, 144411 (2006).  
<sup>77</sup>T. R. Kirkpatrick and P. G. Wolynes, *Phys. Rev. A* **35**, 3072 (1987); *Phys. Rev. B* **36**, 8552 (1987); T. R. Kirkpatrick, D. Thirumalai, and P. G. Wolynes, *Phys. Rev. A* **40**, 1045 (1989); T. R. Kirkpatrick and D. Thirumalai, *Phys. Rev. Lett.* **58**, 2091 (1987).  
<sup>78</sup>W. Kauzmann, *Chem. Rev. (Washington, D.C.)* **43**, 219 (1948).  
<sup>79</sup>C. Chamon, *Phys. Rev. Lett.* **94**, 040402 (2005); C. Castelnovo, C. Chamon, C. Mudry, and P. Pujol, *Phys. Rev. B* **72**, 104405 (2005).

- <sup>80</sup>P. Chandra, P. Coleman, and I. Ritchie, *J. Phys. I* **3**, 591 (1993).
- <sup>81</sup>J. S. Gardner, G. Ehlers, S. T. Bramwell, and B. D. Gaulin, *J. Phys.: Condens. Matter* **16**, S643 (2004).
- <sup>82</sup>F. Ladieu, F. Bert, V. Dupuis, E. Vincent, and J. Hammann, *J. Phys.: Condens. Matter* **16**, S735 (2004).
- <sup>83</sup>D. Bono, P. Mendels, G. Collin, N. Blanchard, C. Baines, and A. Amoto, *J. Phys.: Condens. Matter* **16**, S817 (2004).
- <sup>84</sup>S. Nakatsuji, Y. Nambu, H. Tonomura, O. Sakai, S. Jonas, C. Broholm, H. Tsunetsugu, Y. Qiu, and Y. Maeno, *Science* **309**, 1697 (2005).
- <sup>85</sup>F. Pollmann, P. Fulde, and E. Runge, *Phys. Rev. B* **73**, 125121 (2006); F. Pollmann and P. Fulde, *Europhys. Lett.* **75**, 133 (2006); F. Pollmann, J. J. Betouras, K. Shtengel, and P. Fulde, *Phys. Rev. Lett.* **97**, 170407 (2006); F. Pollmann, J. J. Betouras, E. Runge, and P. Fulde, cond-mat/0609122 (unpublished).